





Ives Iwamoto first author 1981-1989 Newby Herron Dryden Reichert Lin Hlady Reinecke Winterton Stoker Suci Dryden King Van Wagenen Mo

ck View Arrange By Action Share Edit Tags

me	^	Date Modified	Size	Kind
 Ives 1987 TIRF Sensors in Chester bk Reichert Lin Hlady Reinecke Suci Van Wagenen Newby Herron Dryden.pdf		10/11/06	1.1 MB	PDF D
 Ives 1988 Waveguides SPIE.pdf		10/11/06	920 KB	PDF D
 Ives 1989 Fiber Optic IA Review.pdf		10/11/06	1.7 MB	PDF D
 Iwamoto 1981 RFGD Dwight book king.pdf		7/14/06	2.1 MB	PDF D
 Iwamoto 1982 Insulin Tyrosine TIRF van wagenen.pdf		7/14/06	1.1 MB	PDF D
 Iwamoto 1985 Fibronectin Ads winterton stoker van wagenen mosher.pdf		7/14/06	1.5 MB	PDF D

3) The optical fibers are permanently fixed in place, such that the detector sub-assembly becomes a compact and rugged unit.

This approach also appears to offer the benefits of further reduction in scale, by simply reducing the size of the template wire (and perhaps the optical fibers). Sub-nanoliter detector volumes thus appear feasible. It also appears that other configurations of the fibers could be constructed for other types of optical detectors.

¹F.J. Yang, J. High. Resol. Chromatogr. 4 (1981) 83.

²J.W. Jorgenson and K.D. Lukacs, Anal. Chem. 53 (1981) 1298.

³F.M. Everaerts, J.L. Beckers, and Th.P.E.M. Verheggen, *Isotachopheresis*, (Elsevier, Amsterdam, 1976), p. 164.

Total Internal Reflection Fluorescence Surface Sensors.

J.T. Ives, W.M. Reichert, J.N. Lin, V. Hlady¹, D. Reinecke, P.A. Suci, R.A. VanWagenen, K. Newby, J. Herron, P. Dryden and J.D. Andrade

University of Utah Department of Bioengineering, Salt Lake City, Utah 84112 USA

¹Institute "Ruder Boskovic", Zagreb, Yugoslavia

1. Introduction.

Total internal reflection fluorescence (TIRF) technique shows potential as the basis of a remote fluorimmunoassay design (1,2). Evanescent excitation of fluorescently labelled antigens (Ag) complexed with surface immobilized antibodies (Ab), or vice versa, significantly simplifies the rinsing required in standard immunoassay techniques, and allows smaller sample volumes to be measured. The development of integrated waveguide optics as an evanescent spectroscopic technique has opened the possibility of optically detecting interfacially bound biological molecules in remote environments. This paper will review the research at the University of Utah on a remote fiber optic immunosensor and a polymer thin film evanescent sensor. We will also discuss the basic TIRF system as applied to the study of proteins at interfaces because it represents evanescently excited spectroscopy in its simplest form.

2. Fixed Angle TIRF.

Several groups have used total internal reflection in the fluorescence mode to study protein adsorption-desorption reactions (3). The total internal reflection fluorescence of interfacially bound proteins may be monitored intrinsically in the ultraviolet by exciting the tryptophan moieties or extrinsically in the visible using fluorescent labeling techniques. In either case, the fluorescence of the adsorbed protein is excited by an exponentially decaying optical field created immediately adjacent to a solid-liquid interface oriented at such an angle to totally reflect an incident light beam. This exponentially decaying field, commonly called the "evanescent wave", produces a fluorescence excitation volume extending from the

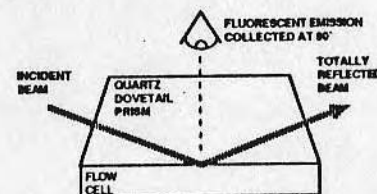


Fig. 1. SCHEMATIC OF FIXED ANGLE TIRF SYSTEM USED TO STUDY PROTEINS ADSORBED TO THE SOLID-LIQUID INTERFACE.

in Optical Fiber Sensors

A.N. Chester, et al, eds.

M. Nijhoff, Publ., 1987

surface of the total reflection element (typically a 70 degree quartz dovetail prism) into the adjacent liquid medium to an effective depth of $1/3$ of the exciting wavelength. The liquid phase is generally contained within a flow cell for the controlled introduction of biological molecules to the totally reflecting interface. The basic TIRF design is displayed in Figure 1 and described in detail in (3,4).

TIRF has been used extensively in our laboratory for several years to study the fluorescence of interfacially bound proteins(3,4). Recently, we have used TIRF as an immunosensor to follow interfacial antigen (Ag)-antibody (Ab) reactions (5).

3. Variable Angle TIRF

Variable angle TIRF (VA-TIRF) is a method to obtain the concentration and thickness of an adsorbed fluorescent layer. The advantage of VA-TIRF over fixed angle TIRF is that one is not required to assume a thickness or refractive index of the adsorbed film when attempting to obtain quantitative data. The concentration-distance profile of fluors at the interface results directly from the numerical inverse Laplace transform of the fluorescence angular spectrum representation where one of the two angles (observation or incident) is varied while the other angle is held fixed (6). In our experimental design a fluorescence curve is obtained by holding the angle of incidence constant and collecting the angular distribution of the interfacial fluorescence by varying the angle of observation (Fig. 2). The VA-TIRF technique in the variable observation angle mode was demonstrated by the collection and numerical analysis of data from an immunoglobulin (IgG) protein film adsorbed to a quartz hemi-cylinder (7). Currently we are testing the accuracy and reliability of the optics and inversion software by collecting spectra of dye impregnated Langmuir-Blodgett monolayers of known thickness and dye concentration (8). In addition to determining the concentration-distance profiles of adsorbed protein layers we are also planning to use VA-TIRF to detect the step increase in thickness when an Ag from solution is complexed with a preadsorbed Ab monolayer producing a bilayer at the prism surface.

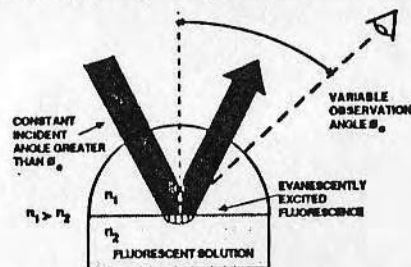


FIG. 2. VARIABLE OBSERVATION ANGLE TIRF (VA-TIRF) SYSTEM FOR DETERMINING THE CONCENTRATION-DISTANCE PROFILES OF ADSORBED PROTEIN MOLECULES TO THE SOLID-LIQUID INTERFACE.

4. Waveguide TIRF.

Waveguide TIRF shows promise as a remote surface sensor to monitor protein adsorption-desorption reactions and Ag-Ab complex formation. The waveguides used in our laboratories to date have been cylindrical glass optical

fibers and 1-3 μ m transparent polymer films spun-cast onto pyrex or glass substrates. Both of these systems utilize an integrated optics modification of the evanescent excitation principle of the conventional total internal reflection geometry.

The evanescent field at the surface of approximately 2 μ m thick spun-cast poly(styrene) films have been used by our group to excite the fluorescence of Langmuir-Blodgett deposited cyanine dye-fatty acid derivative monolayers (9) and surface adsorbed films of dye labeled IgG (10). Figure 3 is an illustration of the prism technique used to couple guided waves of light into thin polymer film. The fluorescence from the surface deposited fluorescent monolayers is collected at 90° to the polymer film surface.

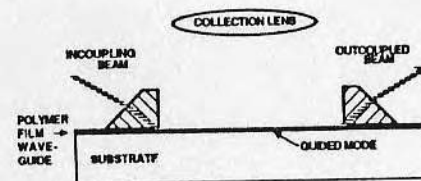


FIG. 3. PRISM TECHNIQUE FOR COUPLING GUIDED MODES OF LIGHT INTO SPUN-CAST POLYMER THIN FILM WAVEGUIDES. THE EVANESCENT FIELD AT THE POLYMER SURFACE IS USED TO EXCITE THE FLUORESCENCE OF SURFACE DEPOSITED LAYERS.

Cylindrical glass waveguides have also been used in our labs as an evanescent surface sensor. A sensor tip is formed by stripping the cladding from one end of a multi mode fiber (600 μ m) and capping the terminal end with an opaque epoxy to prevent light leakage out of the fiber tip into the sample solution (Fig. 4). In this design only the evanescent field of the stripped fiber tip is exposed to the surrounding liquid sample solution. The remote operation of the fiber tip sensor has been demonstrated with fluorescent dye solutions (11). The application of this system to the remote detection of protein adsorption was demonstrated with dye labeled IgG (12).

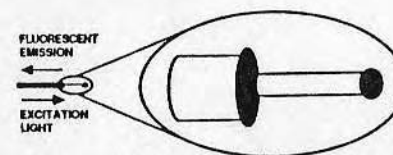


FIG. 4. FIBER SENSOR TIP PRODUCED BY STRIPPING THE CLADDING FROM THE DISTAL END OF AN OPTICAL FIBER. THE EXPOSED FIELD AT THE STRIPPED FIBER CORE SURFACE IS USED TO EVANESCENTLY EXCITE FLUORESCENCE OF MOLECULES ADSORBED TO THE SENSOR TIP.

5. Integrated Optics Based Immunoassay.

Immunoassay systems are widely employed due to their high sensitivity and, with monoclonal antibody techniques, high selectivity (13). In brief, the

immunoassay concept is based on the pre-immobilization of either Ab or Ag to a totally reflecting surface which is exposed to a solution containing the complementary immunospecific species. The observed fluorescence is proportional to the surface concentration of the formed Ag-Ab complexes which is in turn proportional to the concentration of the unbound species in solution. Figure 5 shows a typical fluorescence signal response to pre-immobilized Ab binding with free Ag. When the immobilized Ag is in turn exposed to free Ab the fluorescence signal intensity increases further.

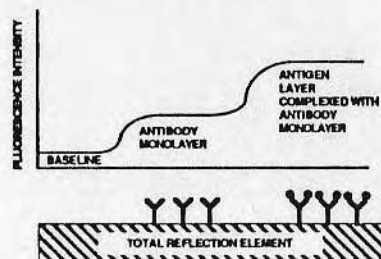


FIG. 6. TIRF IMMUNOASSAY CONCEPT FOR FLUORESCENT ANTIBODY AND ANTIGEN MOLECULES. THE OBSERVED FLUORESCENCE WILL INCREASE ONE STEP WITH THE ADSORPTION OF THE ANTIBODY MONOLAYER FOLLOWED BY A SECOND STEP INCREASE AFTER THE COMPLEXATION OF THE ANTIGEN FROM SOLUTION WITH THE PRE-IMMOBILIZED ANTIBODY LAYER.

Fiber Sensors.

The attractiveness of fiber optic sensors are their small size and ability to deliver and collect light to and from remote locations. The concept of a semi-continuous fiber optic immunosensor utilizing a competitive assay scheme is presented in more detail elsewhere (2). Advancing the fiber optic sensor to an immunosensor requires the stable pre-immobilization of the Ab to the surface of the quartz fiber and a mechanism for regenerating the sensing surface *in situ*.

Surface immobilized Ab molecules which are stable, active, and selective have been obtained using two different techniques. A technique which uses a 3-aminopropyl-triethoxysilane prepared surface has been described by Weetall, et al. (13), and covalent binding on a dimethyldichlorosilane prepared surface has been developed by Lin, et al. (14). Work is being performed on these pre-immobilized surfaces in the TIRF mode to test their potential as affinity surfaces suitable for fluoro-immunoassay.

The current immunoassay techniques are essentially single use techniques. A remote fiber optic immunosensor should include a mechanism for semicontinuous monitoring. We are investigating two methods for long term use based on remote surface regeneration. One method is a photoinduced conformational change in the Ab which causes the Ag to be released. Light at a wavelength other than the fluorescence excitation wavelength is propagated down the optical fiber to induce a change in a photosensitive segment of the Ab. Preliminary work with azobenzene rings on poly-L-glutamic acid has shown a photoinduced conformational change. The second method involves a permanent modification of the Ab binding site to reduce the binding constant. A reduced

binding constant would yield a faster response time of the sensor to fluctuations in the solution Ag concentration.

A number of optical improvements also need to be considered before a suitable immunosensor is developed. Currently, the system is standardized with fluorescent dyes in the test chamber, but future referencing should probably utilize two wavelength or broad band comparisons. The coupling and detection systems are large and expensive (lasers, microscopes, spectrometers, photon counting), and much simpler components (diode lasers operating in the visible wavelengths, fiber optic spectrometers) are needed. Fluorescence is currently used because of its large emission signal offsets (Stokes shift) and quantum efficiency. Improved sensitivity and a tunable source/detector would allow chromophore absorption to be studied with perhaps wider applications than fluorescence. Another important parameter in fluorescence spectroscopy is polarization anisotropy which compares light absorption and emission in two orthogonal polarizations. Only with polarization maintaining fibers can such studies even be considered, but the probability of success is low due the small amount of bound energy in these single mode fibers.

Polymer Thin Film Waveguides.

An alternative to fiber optics are slab waveguides made from spun-cast polymer films. Polymer waveguides potentially have several advantages over optical fibers: 1) the large surface area of polymer waveguides is easily adapted to different surface chemistries (i.e., polar vs. nonpolar, hydrophilic vs. hydrophobic, mobile vs. rigid) through the use of different polymer films or surface derivatization, 2) the mode and polarization can be selected for different effects at the polymer film surface, and 3) the linear shape of the waveguide streak is efficiently imaged onto the spectrometer slit (3). The disadvantages of a thin film sensor are the scatter loss along the polymer film and the bulky prism system used to couple light into the waveguide.

Fluorescence excitation caused by the scattered field represents a large noise factor in the detected signal. Waveguide features of evanescent surface selectivity and mode selection of different excitation volumes become difficult to distinguish above the background scatter. This problem is being approached with calculated energy profiles of four layer waveguide systems (substrate-waveguide-film-superstrate), theoretical absorption and scatter losses and experimental work measuring the decay of light along the waveguide. Scatter caused by the Langmuir-Blodgett surface films and the ability to vary their absorption will be an important part of this study.

The first generation polymer film sensor involves a flow cell designed for the waveguide surface. This design allows protein adsorption and desorption and Ag-Ab reactions to be studied at the polymer surface. The second generation sensor will incorporate the remote sensing advantages of the fiber optics while retaining the surface chemistry and optics advantages of polymer waveguides to produce the optimum immersible sensor. In this design, fiber to waveguide coupling (15) will be used to create an evanescent streak along the polymer waveguide sensing surface (Fig. 6).

6. Summary.

Evanescent wave spectroscopy in the TIRF mode has several advantages for biomedical surface studies (1-3). When coupled with optical fibers and polymer waveguides, remote surface sensitive sensors can be developed for immunoassay measurements and protein adsorption studies. With the techniques reviewed in this paper, information has been obtained

about protein adsorption and desorption kinetics, conformational changes of adsorbed proteins, surface immobilized fluorescent immunoassays, and surface monolayer fluorescence.

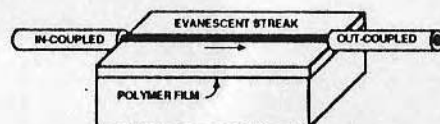


FIG. 6. SCHEMATIC OF FIBER TO POLYMER FILM WAVEGUIDE COUPLING WHICH WOULD INCREASE THE SUITABILITY OF THIN FILM WAVEGUIDES FOR REMOTE SENSOR APPLICATIONS.

7. References.

1. Place, J.F., R.M. Sutherland and C. Dahne, "Opto-Electronic Immunosensors: A Review of Optical Immunoassay at Continuous Surfaces", *Biosensors*, **1**, 321-353 (1985).
2. Andrade, J.D., R.A. Van Wagenen, D.E. Gregonis, K. Newby and J-N Lin, "Remote Fiber Optic Biosensors Based on Evanescent Excited Fluoro-immunoassay: Concept and Progress," *IEEE Trans Electr Dev*, ED-32, 1175-1179 (1985).
3. J.D. Andrade, ed., *Surface and Interfacial Aspects of Biomedical Polymers*; Vol 1: *Surface Chemistry and Physics*, Vol. 2: *Protein Adsorption*, Plenum Press, New York (1985).
4. Hlady, V., Reinecke, D.R., and J.D. Andrade, "Fluorescence of Adsorbed Protein Layers. 1. Quantitation of Total Internal Reflection Fluorescence," *J Coll Interface Sci*, **111**, 555-569 (1986).
5. Lin, J-N., V. Hlady, W.M. Reichert and J.D. Andrade, "Immunosensors Based on Evanescent-Excited Fluorescence", *Annual Meeting of the Electrochemical Society*, Las Vegas, Oct., 1985.
6. Sansone, M., F. Rondelz, D.G. Peiffer, P. Pinus, M.W. Kim and P.M. Eisenberger, "Concentration Profile of a Dissolved Polymer near the Air-Liquid Interface: X-Ray Fluorescence Study", *Phys Rev Lett*, **54**, 1039-1042 (1985).
7. Suci, P.A. "Variable Angle Total Internal Reflection Fluorescent Spectroscopy", Masters Thesis University of Utah 1984.
8. Suci, P.A., W.M. Reichert, J.T. Ives and J.D. Andrade, "Variable Angle Total Internal Reflection Fluorescence", *Annual Meeting of the Society for Biomaterials*, Mpls, May, 1986.
9. Ives, J.T. W.M. Reichert, P.A. Suci and J.D. Andrade, "Waveguide Evanescent Streak Excitation of Surface Deposited Dye Monolayer Fluorescence," *J. Opt. Soc. Am.*, **A2(13)** (1985), p.53
10. Reichert, W.M., K. Newby and J.D. Andrade, "Waveguide Evanescent Streak Excitation of Adsorbed Protein Fluorescence," *Annual Meeting of the Society for Biomaterials*, April 1985.
11. Newby, K., W.M. Reichert, J.D. Andrade and R.E. Benner, "Remote Spectroscopic Sensing of Chemical Adsorption Using a Single Multimode Optical Fiber," *Appl Optics*, **23** 1812 (1984).
12. Newby, K., J.D. Andrade, R.E. Benner and W.M. Reichert, "Remote Sensing of Protein Adsorption Using a Single Mode Optical Fiber," *J. Colloid Interface Sci.*, **111** (1986), pp 280-283.
13. H.H. Weetall, ed., *Immobilized Enzymes, Antigens, Antibodies and Peptides*, Plenum Press (1975).
14. Lin, J-N., J.N. Herron and J.D. Andrade, in preparation.
15. Bear, P.D. "Microlenses for Coupling Single-Mode Fibers to Thin Film Waveguides", *Appl. Optics*, **19**, 2906-2909 (1980).

ABSTRACT

The evanescent and scattered light from poly(styrene) thin film waveguides are being investigated to evaluate the potential use of integrated optic waveguides as sensors. A fiber optic system is described for measuring the light intensity of different waveguide modes in two directions; perpendicular to the waveguide streak and parallel to the streak as a measure of decay. Rayleigh and poly(styrene) Raman scattered light are used as intensity indicators and the advantages and disadvantages of each are discussed. Profiles of Raman scattered light across the waveguide streak are shown as a function of position along the waveguide. Decay measurements of four waveguide modes along a single waveguide are divided into three regions with different rates of decay and possible causes. These results show that the excitation field along the surface of IO waveguides is predominantly scattered light rather than surface localized evanescent light.

1. INTRODUCTION

Due to boundary conditions at the waveguide/substrate interface, light propagating as a bound mode within an integrated optics (IO) slab waveguide creates an evanescent streak along the waveguide surface. This evanescent streak decays exponentially in the substrate and superstrate media with a penetration depth (1/e amplitude decay) of approximately 1000Å. The evanescent streak of IO waveguides has been used to excite Raman scattering from thin polymer films¹, fluorescence and Raman emission from Langmuir-Blodgett monolayers^{2,3}, fluorescently labelled molecular layers⁴ and CARS spectroscopy of adsorbed molecular layers⁵. In addition to the evanescent field, several other features make IO waveguides attractive as interfacial optical sensors: high intensity, large signal area, polarization control, mode selection and potential integration into hybrid optical/electrical systems.

The interfacial field of single reflection prisms⁶ and thin film slab waveguides⁷ has been shown to consist of scattered light in addition to evanescent light. Figure 1 from Reichert et al.⁷ shows the relative contributions of the evanescent and scattered light to excite fluorescence within a 0.51mm thick flow cell on a poly(styrene) waveguide. This plot is calculated from expressions fit to experimental data. The data was obtained by injecting increasing concentrations of fluorescein dye into the flow cell and collecting the fluorescence emission. The cross hatched region is emphasized to illustrate that with experimentally reasonable concentrations ($cc \leq 1$), the scatter excited component is much larger than the almost insignificant evanescently excited fluorescence. From these results, the use of IO polymer waveguides as surface sensors, particularly in the presence of fluorescing bulk media or solutions, will require methods to separate the scatter and evanescent components, or will require IO waveguide sensors to be considered primarily as scatter sensors. A common method to determine waveguide losses due to scatter is to monitor the intensity decay of a propagating waveguide mode. In this report, we describe a fiber optic system used to measure the longitudinal decay and transverse profile of different waveguide modes. Preliminary results obtained with the fiber optic system will be presented. The relevance of these waveguide measurements to characterizing the optical field at the waveguide surface will be discussed.

2. METHODS

Waveguides were spun cast from 10% (weight/volume) solutions of poly(styrene) (secondary standard, $M_n = 84600$, Aldrich) dissolved in spectral grade chlorobenzene (Aldrich). Prior to dissolving in chlorobenzene, residual styrene monomer was separated from the poly(styrene) by a repeated (3x) toluene/methanol solvation/precipitation sequence. The remaining toluene and methanol solvents were removed by oven drying at 80°C for 12 hours. The purified poly(styrene)-chlorobenzene solution was spun cast onto acid cleaned quartz slides (1"x3", ESCO Products) with a Headway photoresist spinner. The polymer films were dried for 4 hours at 110°C and stored in sealed, acid cleaned jars.

TE polarized 488nm light from an argon ion laser (Lexel Model 95) was coupled into the waveguide with LaSF₆ right angle prisms (Ohara Optical Glass). The mode coupling angles were precisely selected by adjusting the position and angle of the x,y,z stage-goniometer mount (Rigaku X-Ray) supporting the prism-waveguide assembly. Light collected from the flow cell or waveguide was then coupled into a scanning monochromator (Instruments SA, Inc. HR-640) with 1mm entrance and exit slits. The flow cell and specific collection equipment for the fluorescein dye solutions and protein experiments is described in Reichert et al.⁷ and Ives et al.⁴, and the collection equipment for the decay characterization of waveguide modes will be described below. The monochromator output was detected with a Hamamatsu R585 photomultiplier tube and Eg&G Ortec photon counting instrumentation. A 488nm blocking filter (Pomfret) placed before the monochromator entrance allowed Rayleigh scattered light to be measured without photomultiplier tube saturation.

The refractive index and thickness of each waveguide was determined using the coupling angle technique developed by Swalen et al.⁸ modified by the collection of Rayleigh or Raman scattered light from the waveguide.

2.1. Waveguide characterization (Figure 2)

Two different spectroscopic signals, Rayleigh scatter at 488nm and poly(styrene) Raman emission around 513nm, were used to monitor the longitudinal decay and transverse profile of the propagating waveguide modes. The emission signals were collected with a 200µm diameter quartz optical fiber (Quartz Products) held by a fiber optic positioner (FP-2, Newport) on an x,z stage with micrometer drives (Newport). The end of the optical fiber was positioned next to the quartz slide approximately 2mm from the poly(styrene) waveguide. To ensure that the optical fiber moved parallel to the waveguide surface, the optical fiber and its reflected image were viewed in a dissecting scope using the scattered waveguide light for illumination. The spacing between the fiber and the reflected image was adjusted to be constant (maximum deviation from parallel < 1°) across the measurement region using the tilt adjustments on the fiber optic positioner. The fiber optic output was coupled into the Instruments SA, Inc. monochromator with a collection and collimating lens (F3.8) and a focussing lens (F6.5). Individual data points on Figures 3 - 6 are obtained by averaging fifty 1 second counts from the photon counting system.

3. RESULTS

A profile of the light intensity across a waveguide (thickness = 1.78µm, refractive index = 1.58), transverse to the direction of propagation, is shown in Figure 3 for both Rayleigh scattered light at 488nm and poly(styrene) Raman emission around 513nm. The irregular Rayleigh scattered signal occurs because the Rayleigh signal is a direct result of scattering sites which are not necessarily uniformly distributed. Raman emission from the poly(styrene) directly indicates the light intensity within the waveguide and is relatively insensitive to individual scattering sites. For similar reasons, Miller et al.⁹ also use Raman emission for waveguide characterization. The relatively low Raman scattering signal can be partially overcome with large slit widths as was done in these experiments (1mm slit width, approximately 1.5nm resolution). This is particularly successful with poly(styrene) around 513nm because there are several Raman peaks in this area which sum to enhance the Raman signal. The remaining waveguide characterization figures in this report will display the poly(styrene) Raman signal only.

Figure 4 displays transverse profiles of waveguide Raman scattering measured at four positions along a decaying v 2.07µm, refractive index = 1.58). These measurements were obtained with the zeroth order ($m = 0$) mode coupled, but very 2 and 3 modes. This preliminary data indicates that the waveguide energy is confined to a constant width waveguide background light intensity off the main streak axis. Therefore, measuring the peak light intensity along the length of the accurate indicator of waveguide intensity decay.

The decay measurements for each mode in the waveguide used in Figure 4 are plotted on a linear scale in Figure 5 with the curves for each mode normalized and offset for visual clarity. The data were obtained by optimizing the coupling angle for a specific mode and then moving the 200µm fiber across the waveguide streak to determine the peak Raman signal at several positions along the length of the waveguide. The $m = 1$ mode intensity peak around 16 mm is presumably due to the large slit widths and therefore poor monochromator rejection of the Rayleigh scattered light.

4. Discussion

Protein adsorption experiments on poly(styrene) thin film waveguides⁴ are qualitative demonstrations of sensing by IO waveguides. However, attempts to quantify the results and determine the surface concentration of the adsorbed protein molecules without correcting for the scatter excitation component are extremely inaccurate⁴. Hlady et al.⁶ have developed a quantitation method for a single internal reflection technique, total internal reflection fluorescence (TIRF). Their quantitation method emphasizes the importance of separating the fluorescence emission excited by scattered light from that excited by evanescent light. To improve our understanding of the IO waveguide evanescent and scatter components, we have begun characterizing the longitudinal decay and transverse profile of light propagating within poly(styrene) waveguides.

The measured intensity within a uniformly scattering waveguide would decay as an exponential with the decay rate depending upon the surface roughness, refractive index variations, scattering sites and waveguide mode. Therefore, a useful way to plot decay data is to plot the decibel (dB) values, i.e., $10 \cdot \log(\text{signal})$, vs the distance¹⁰. A uniformly scattering waveguide would plot as a straight line with the slope indicating the decay rate, often quoted in dB/cm. In Figure 6, the data of Figure 5 is replotted as dB vs longitudinal position. The data is clearly not a straight line over the entire measuring distance. To develop a preliminary explanation of these results, we have divided Figure 6 into three regions.

In the region closest to the incoupling prism, the light within the waveguide is composed of propagating bound modes confined within the waveguide by total internal reflection and radiative modes traveling at angles less than the critical angle but with high reflectivity at the waveguide-substrate interface. The first three data points of the $m = 0, 2$ and 3 mode curves of Figures 5 and 6 indicate a slightly greater decay rate which may be due to radiative mode losses. Measurements closer

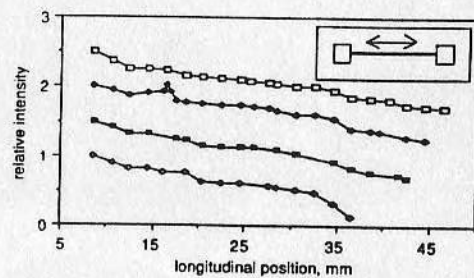


Figure 5. Decay measurements for four waveguide modes. The peak intensity of the poly(styrene) Raman signal was measured in approximately 2mm increments along the waveguide. The symbol in the upper right indicates the direction of optical fiber movement. The individual mode curves have been normalized by the signal at 8.5mm, and shifted for clarity. Mode 0 = white squares; Mode 1 = black diamonds; Mode 2 = black squares; Mode 3 = white diamonds.

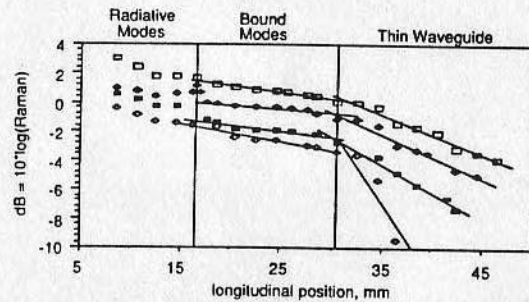


Figure 6. Decibel (dB) plot of waveguide decay data in Figure 5. Three regions of waveguide decay are identified; Radiative Modes, Bound Modes and Thin Waveguide. Least squares fit lines to the data points in the Bound Mode and Thin Waveguide regions are used to determine the slope and therefore decay rate as a function of waveguide mode. The curves for each mode are normalized by the 8.5mm value and shifted for clarity. Mode 0 = white squares; Mode 1 = black diamonds; Mode 2 = black squares; Mode 3 = white diamonds.

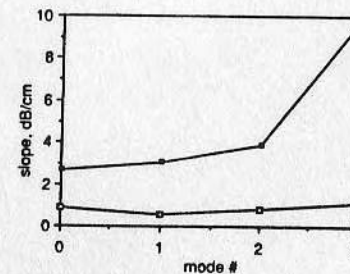


Figure 7. Decay rates as a function of mode number. The decay rates are the slope of the least squares fit line to each mode in Figure 6. The "Thin Waveguide" region of Figure 6 is indicated by the black squares, and the "Bound Mode" region by the white squares.

to the incoupling prism may indicate this loss more clearly. The $m = 1$ mode data does not follow the pattern of the other modes, but the intensity peak around 16mm may have affected the decay measurements in this region.

The mode decay curves in the midsection of this waveguide, from approximately 17mm to 29mm, have been fit (least squares analysis) with a straight line as shown in Figure 6. The waveguide streak in this region appeared visually as a bright narrow line with little intensity decrease. The streak appearance is consistent with the relatively low slope of the mode curves, approximately 1 dB/cm. However, the decay rates do not increase with mode number as we expected (Figure 7). Based on the readily observed Newton diffraction rings in the waveguides, surface roughness was assumed to be a major cause of waveguide scattering losses. The lowest order $m = 0$ mode is most confined to the waveguide medium and has the lowest percentage of its energy in the evanescent field. This mode is presumably the least affected by surface roughness. Therefore, it was expected that the $m = 0$ mode would have the flattest slope with an increasing progression to the highest decay rate for the highest order mode.

The waveguide streak in the third region of Figure 6 appeared to significantly decay in intensity, and this visual appearance was consistent with the steep decay rates in Figures 6 and 7. The rapid decay was most obvious for the $m = 3$ mode, where decay measurements were not continued beyond 36.5mm due to the low intensity of the waveguide Raman signal. In this region, the relative decay rates support the opinion that scatter losses increase with mode number (Figure 7).

The change in decay rates between the midsection and end regions of the waveguide may be due to uneven waveguide thickness. The waveguides were fabricated by spin casting on rectangular 3"x1" slides. The circular spin casting results in an uneven distribution of polymer on the slide, creating a thinner, perhaps more lossy, waveguide on the ends. Alternative methods of fabricating polymer waveguides, such as dip casting, may create more uniform waveguides⁹.

5. CONCLUSION

The measured decay rates of these spun cast polymer waveguides appear to support the idea that a large percentage of the excitation light in a polymer waveguide-flow cell experiment is scattered light. In a relatively low loss polymer waveguide of 1dB/cm, approximately 20% of the incident light is scattered out of the waveguide in a 1cm distance. The evanescent field, on the other hand, is approximately 2% or less of the total waveguide energy at any single location. Our current efforts include integrating these two pieces of information into an indicator of the evanescent/scatter ratio. From such information, we can evaluate the use of spun cast polymer waveguides, or the potential use of low loss sputtered glass waveguides, as IO waveguide surface sensors, or accept the existence of a scatter sensor.

6. ACKNOWLEDGEMENTS

Funding for this project was provided by NIH grant HL32132, a seed grant from the Center for Sensor Technology at the University of Utah and by a Biomedical Research grant from the Whitaker Foundation. We would also like to thank D. Yoshida, P. Suci and D. Christensen for helpful discussions and technical assistance.

- ¹ J.F. Rabolt, N.E. Schlotter, J.D. Swalen and R. Santo, J. Polymer Sci. 12, 1 (1983).
- ² J.F. Rabolt, R. Santo, N.E. Schlotter and J.D. Swalen, IBM J. Res. Develop. 26, 209, (1982).
- ³ J.T. Ives, W.M. Reichert, P.A. Suci and J.D. Andrade, J. Opt. Soc. Am. A2, 53 (1985).
- ⁴ J.T. Ives, P.A. Suci and W.M. Reichert, Appl. Spectr., January 1988, in press.
- ⁵ W.M. Helmerington and G.I. Stegeman, Chem. Phys. Lett. 126, 150 (1986).
- ⁶ V. Hlady, D. Reinecke and J.D. Andrade, J. Coll. Interface Sci. 111, 555 (1986).
- ⁷ W.M. Reichert, J.T. Ives, P.A. Suci and V. Hlady, Appl. Spectr. 41, 636 (1987).
- ⁸ J.D. Swalen, M. Tacke, R. Santo, K.E. Rieckhoff and J. Fischer, Helv. Chimica Acta 61, 960 (1978).
- ⁹ D.R. Miller, O.H. Han and P.W. Bohn, Appl. Spectr. 41, 245 (1987).
- ¹⁰ K. Tiefenthaler, V. Brigue, E. Buser, M. Horisberger and W. Lukosz, SPIE 401 (1983).

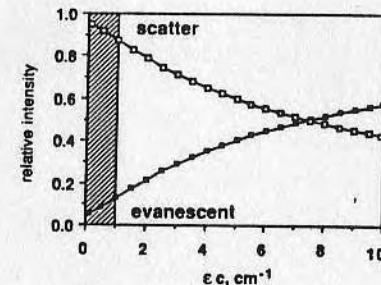


Figure 1. Evanescent and scatter excitation components in a waveguide-flow cell experiment. The curve is taken from Reichert et al., 1987 (ϵ is the extinction coefficient, c is the concentration). The cross hatched region indicates the area of experimentally reasonable ϵc values.

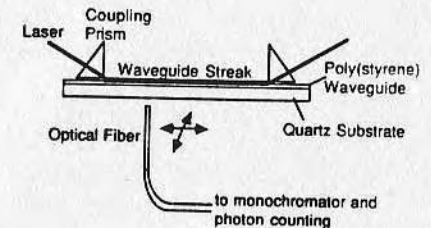


Figure 2. Fiber optic measurement system. The 200 μ m diameter optical fiber can be scanned perpendicular to the waveguide streak or parallel to the streak with x, z micrometer stages. See text for more details.

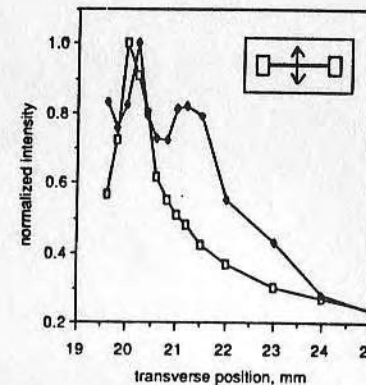


Figure 3. Rayleigh vs Raman scattered light as a waveguide intensity indicator. Fiber optic collection across the waveguide streak as indicated by the figure in the upper right. Rayleigh (488nm) = black diamonds; Raman (513nm) = white squares.

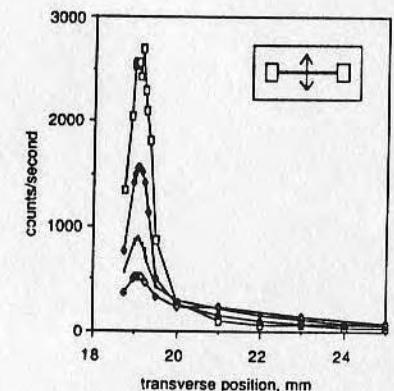


Figure 4. Raman intensity profiles at different locations along waveguide streak. Fiber optic collection across waveguide at 8.5mm (white squares), 24.5mm (black triangles), 38.5mm (black squares) and 46.5mm (white triangles).

Fiber-optic fluorescence immunosensors

BY J.T. IVES, J.N. LIN, AND J.D. ANDRADE

IMMUNOASSAYS ARE analytical techniques based on an immunological reaction. With the introduction of competitive radioimmunoassay (RIA) by Yalow and Berson in the 1950s, detection of very low concentrations of antigens (Ags) or antibodies (Abs) became practical.¹ Although both high sensitivity and specificity are obtained, there are several disadvantages with RIA. Health hazards, disposal difficulties, and short shelf life are the most troublesome problems of using radioisotopes. Therefore, nonisotopic labels have been sought to substitute for radioisotopes. Enzymes and fluorescent molecules are the most popular alternative labels. Both heterogeneous (separation steps required) and homogeneous (no separation) types of enzymeimmunoassay (EIA) and fluoroimmunoassay (FIA) have been developed and are being used more frequently in the clinical laboratory.

Furthermore, because of recent progress in immunology and biotechnology, especially with the advent of monoclonal Ab (MAb) techniques, it is possible to produce a wide range of pure Abs against an almost unlimited number of Ags. During the late 1970s, an explosive growth occurred in the application of immunoassay to other biomedical fields as well as to nonbiomedical areas, such as agriculture and environmental monitoring.

Although conventional immunoassays are powerful analytical techniques, they are subject to several limitations. They are slow and require trained technicians to conduct the tests in a centralized laboratory. The delay in obtaining results could cause inconvenience or even a serious problem to the patient's safety. Therefore, it is desirable for physicians to be able to directly, quickly, and continuously monitor the change in analyte concentration.

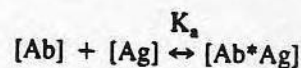
Since the early 1980s, considerable research efforts have been devoted to the development of optical fluoroimmunosensors because 1) the sensitive FIA can be easily used in sensor mode; 2) the apparatus can be designed such that the assay can be performed by nontrained people without a dedicated laboratory; 3) the reagents required for the assay can be prepacked in the sensing element to provide fast and continuous measurements; 4) the optical element transmits light

efficiently, thus it has the ability for remote sensing; 5) the assay has the potential for in vivo monitoring due to the ease of miniaturization; and 6) the optical waveguide can be designed for multichannel sensing. Current results indicate that optical immunosensors may well be a substitution which will provide better service than conventional immunoassays in many situations.

This article discusses the principles of immunoassays and optics for immunosensing. Different strategies for designing the sensors will be briefly reviewed with specific examples from the literature.

Background

The binding of an Ag to an Ab takes place by formation of multiple noncovalent bonds between the antigenic determinant and the Ab active site. The attractive forces include hydrogen bonding, electrostatic, Van der Waals, and hydrophobic interactions and are critically dependent on the distance between the interacting groups. This means that the shape of the Ab active site must fit the antigenic determinant to give significant attractive forces between the two. Thus Ab-Ag binding shows a high degree of specificity. Also, since the noncovalent bonds are dissociable, Ab-Ag reactions are reversible and the Law of Mass Action can be applied. If $[Ag]$ and $[Ab]$ denote the concentration of free Ag and Ab, respectively; and $[Ab*Ag]$, the Ab-Ag complex concentration; then the equilibrium binding expression is given by:



where K_a is the affinity for binding a monovalent Ag to an Ab. The magnitude of K_a indicates the strength of individual Ab-Ag binding.

Competitive FIA is widely used in the detection of Ab-Ag reactions and has been applied to the development of optical immunosensors. It can be performed in two different ways. In the first case, the Ab is immobilized on a solid surface followed by exposure to an Ag solution (Figure 1a). Labeled Ag (fixed concentration) and unlabeled Ag (standard or unknown) in the solution compete with each other for a constant and limited number of Ab active sites. With increasing amounts of unlabeled Ag, the amount of labeled Ag bound to Ab will decrease. After a separation to remove the free Ag signal, the bound and labeled Ag functions as a tracer for determining the total Ag concentration.

In the second case, the immobilized Abs are pre-

The authors are with the Department of Bioengineering, College of Engineering, University of Utah, Salt Lake City, Utah. The authors' work on fluoroimmunosensors is being supported by the US Army Research Office (Contract ARO 25539-LS) and by National Institutes of Health (Grant HL 37046).

Amer Bio Tech Lab

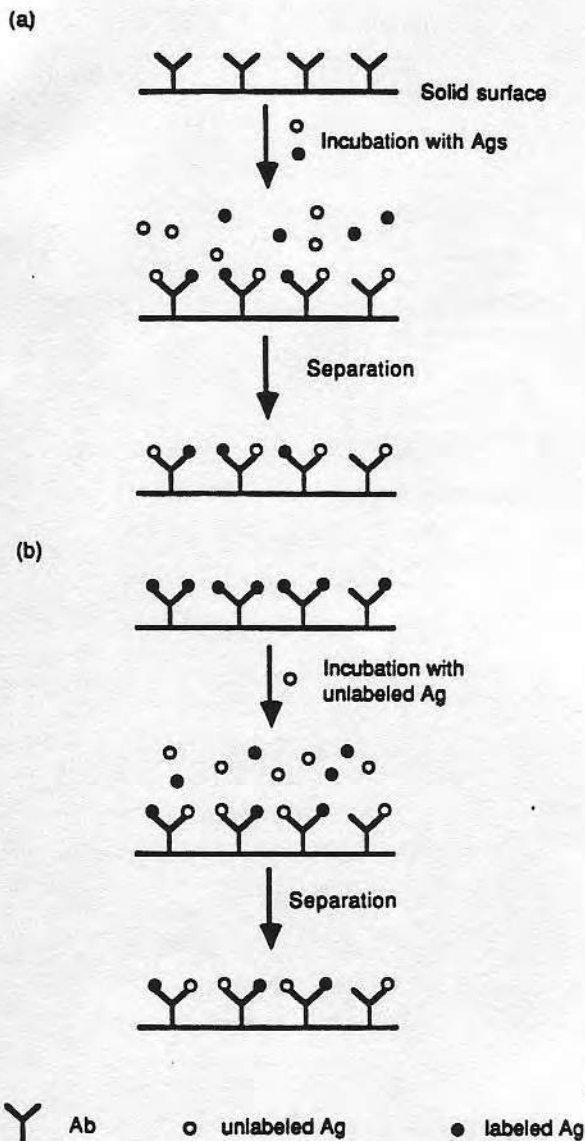


Figure 1 Schematic of competitive immunoassays: a) direct competition; b) exchanging competition.

loaded with labeled Ags (Figure 1b). In the presence of sample, the labeled Ag is gradually replaced by unlabeled Ag and the degree of exchange at equilibrium depends on the Ag concentration in the sample. However, the rate of exchange or response time is determined by the dissociation rate, k_2 , of the Ab and labeled Ag complex. It has been shown that Abs with high sensitivity (i.e. high K_a) normally have slow k_2 . For the binding of monovalent Ags, such as low molecular weight drugs, the exchange can reach equilibrium within a reasonable response time (15-20 min). On the other hand, when large Ags like proteins with many antigenic determinants are used, k_2 is severely reduced due to multivalent binding and slow diffusion of the Ag. Exchange then becomes an impractical method for an assay.

The assays can also be used to monitor Ab concentration by immobilizing the Ag first, followed by

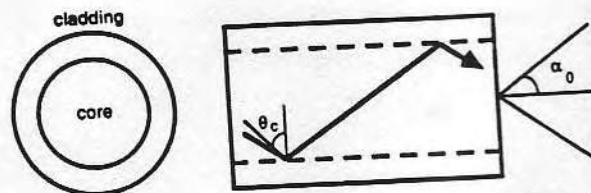


Figure 2 Total internal reflection (TIR) and optical fibers.

incubating the Ag with a solution containing labeled Abs and unlabeled Abs of an unknown concentration.

Competitive EIA is also a widely used technique in conventional assays. However, it is less popular than FIA in the development of optical immunosensors because it requires the addition of chromogenic substrates after Ab-Ag binding. Therefore, it is more difficult to develop a homogeneous immunoassay using EIA.

Optics

An optical fiber generally consists of a cylindrical, transparent core made of glass, quartz, or polymer and a surrounding cladding layer of a lower refractive index (Figure 2). Optical fibers work on the principle of total internal reflection (TIR) where an incident light beam strikes an interface separating a high refractive index dielectric medium 1 (the fiber core) from a lower refractive index dielectric medium 2 (the cladding, Figure 2).² The angle of refraction in medium 2 can be determined from Snell's Law, as follows:

$$n_1 \sin \theta_1 = n_2 \sin \theta_2$$

where the subscripts indicate the medium, n is the refractive index, and θ is the angle of propagation (0° is normal to the interface). When n_1 is greater than n_2 , a specific θ_1 , called the critical angle, can be determined where the light refracted into medium 2 travels directly along the interface (the angle in medium 2 is equal to 90°). The critical angle, θ_c , is defined as,

$$\theta_c = \arcsin(n_2/n_1)$$

For example, the critical angle for light incident from a quartz medium ($n = 1.46$) and reflecting from a water interface ($n = 1.33$) is equal to 65.6° . For incident angles greater than the critical angle, propagating light does not refract into medium 2 and all the light is reflected back into medium 1. Since all the light is reflected, the phenomenon is called total internal reflection. In optical fibers, light travels along angles greater than the critical angle and remains bound within the fiber core by multiple total internal reflections. Total internal reflection allows optical fibers to

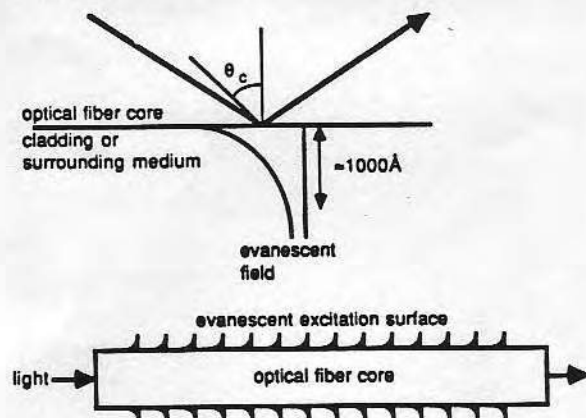


Figure 3 *Evanescent fields. Total internal reflection leads to an exponentially decaying field which penetrates into the lower index medium. Although the lower diagram schematically shows discrete reflection points along the surface of an optical fiber, this is only done for clarity, and the actual evanescent field along an optical fiber is continuous.*

deliver and receive light from distant locations with very low losses. Light which propagates out the terminal end of the cylindrical fiber radiates in a defined cone of emission determined by the critical angle of the fiber and refraction into the terminal medium (Figure 2). Light that is launched into the optical fiber follows the same cone of light. This cone is commonly referred to as the numerical aperture (NA) which is defined in the following equation,

$$NA = n_0 \sin \alpha_0$$

where the subscript 0 indicates the terminal medium and α_0 is the half angle of the emission cone (Figure 2). Fluors located at angles wider than defined by the NA are not excited by light leaving the fiber end, nor is their emission collected by the optical fiber.

Optical fibers utilize TIR to achieve long propagation lengths with very low losses, but another feature of TIR can be used in optical sensing for surface sensitivity. When light is internally reflected from a dielectric interface, the interfacial intensity is not equal to zero. Physical requirements of continuity across an interface result in an exponentially decaying field which penetrates into medium 2 (Figure 3). This field is called the evanescent field. The decay rate of the evanescent field depends upon the incident wavelength, relative refractive indices of medium 1 and 2, and angle of incidence, but for a typical fluoroimmunosensor (quartz optical fiber, visible light), the power decays to one-third of the interfacial value in 500-1000 Å. By removing the cladding to expose the fiber core, the surface localized excitation field can be used to excite fluors close to the surface, rather than in the bulk (Figure 3).

Evanescent fields can also be used to couple a surface-localized fluorescent signal back into the optical fiber where it is guided to a remote detector. This process has been referred to as evanescent coupling, back coupling, reciprocity, and optical tunneling.³ A propagating fluorescent ray from the surrounding low index medium cannot refract at the core

interface and be directed along angles greater than the critical angle. Therefore, bulk fluorescent signals which originate far from the optical sensor cannot be bound within the fiber. However, the evanescent (or near field) emission from fluors close to the interface can couple into guided light much like guided excitation light can create an evanescent excitation field. Thus, evanescent coupling allows remote detection through a surface sensitive filter.

Current fluoroimmunosensor designs

Development of a fiber optic fluoroimmunosensor requires choosing between homogeneous and heterogeneous assay methods, and it also requires a choice between terminal end (transmission) aspects of an optical fiber and surface or evanescent excitation and collection. The following paragraphs illustrate the different combinations of immunoassay chemistry and fiber optics by presenting a brief description of current fluoroimmunosensors.

Transmission mode

Optical immunosensors based on transmission mode to excite labeled molecules and collect fluorescence have been constructed in several ways. One approach

is to immobilize Abs or Ags at the distal face of the optical fiber tip (Figure 4). The sensor is then exposed to labeled and unlabeled Ag or Ab. After washing, the remaining fluorescence intensity is inversely proportional to the unlabeled Ag concentration in solution. This design has been demonstrated by Tromberg et al.⁴ Rabbit immunoglobulin was immobilized (IgG) as an Ag on the fiber tip, and then fluorescein labeled Ab was detected. The advantages are that the sensing surface is easy to prepare and the efficiency of fluorescence collection is high. However, since washing is required, the transmission mode cannot be used for in situ or continuous monitoring.

The second approach is to build a sensing chamber at the sensor tip using a dialysis membrane. The fluorescently labeled Ags are coupled to large molecules and therefore are confined inside the chamber because of the small pore size of the membrane. Antibody in the chamber can complex with the labeled Ag. Unlabeled Ag in the surrounding solution diffuses into the chamber and displaces some of the labeled Ags from the Abs. The free and labeled Ag can be separated optically from the bound and labeled Ag.

This type of sensor has the ability for on-line and continuous monitoring because the labeled Ag inside the sensing compartment always equilibrates with the surrounding unlabeled Ag. The limitation is that the sensor can only be used for the detection of small Ag

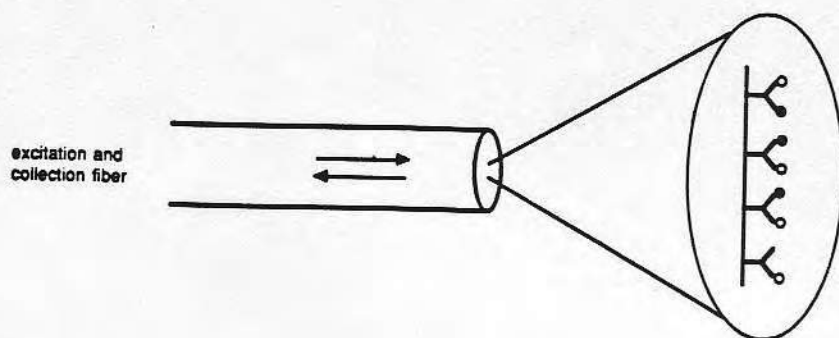
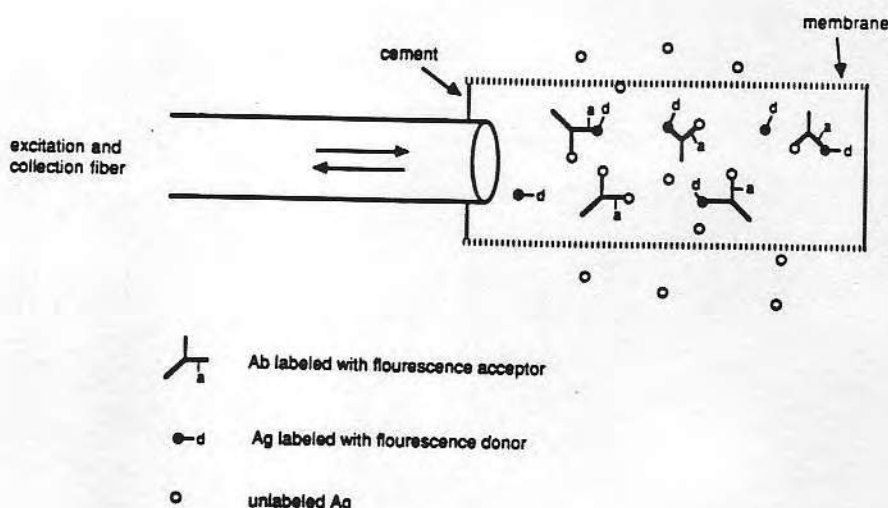


Figure 4 Schematic of an optical fiber immunosensor using distal face of the fiber tip as the sensing element.

Figure 5 Schematic of an optical fiber immunoassay based on energy transfer immunoassay using a dialysis membrane.



molecules, as a result of the small holes on the membrane.

Anderson et al. have developed a sensor based on energy transfer immunoassay using a dialysis membrane at the fiber tip (Figure 5).⁵ Inside the reaction chamber, the Ag, phenytoin, labeled with B-phycoerythrin (fluorescence donor) is bound by the Ab labeled with Texas Red (fluorescence acceptor). When the donor and acceptor are in close proximity, acceptor fluorescence is high and donor emission is low. In the presence of sample, the labeled Ag is exchanged by the unlabeled Ag. As a result, fluorescence from the donor will increase, accompanied by a decrease in fluorescence intensity of the acceptor. The ratio of the donor and acceptor fluorescent signals indicates Ag concentration.

A similar sensor has been demonstrated by Mansouri et al. based on receptor-ligand binding for measuring the level of glucose (Figure 6).⁶ Although a carbohydrate receptor was used in this sensor instead of an Ab, the principle is still applicable to Ab-Ag binding.⁷ The carbohydrate receptor, Concanavalin A (Con A), is immobilized on the inner surface of a dialysis membrane attached to the end of an optical fiber. The sensing element is designed in such a way that the Con A is out of the optical pathway or numerical aperture. The membrane is permeable to glucose but not to high molecular weight fluorescein-labeled dextran that is

confined within the sensing chamber. Glucose in the external solution diffuses through the membrane into the sensing element to compete with the dextran for the binding to Con A. Fluorescence from the unbound dextran diffuses into the excitation/collection cone of the optical fiber, and the fluorescence signal indicates glucose concentration.

Evanescent mode

By using the evanescent surface sensitivity of optical fibers, several researchers are working on homogeneous immunoassay systems. These systems would potentially allow remote detection and continuous monitoring. The basic sensor design (Figure 7) consists of a light source (laser, mercury lamp, or other source consistent with the chosen fluorescent dye), optics for directing the excitation light and collecting the fluorescence (lenses and dichroic, notch and hi-pass wavelength filters), an optical fiber with an exposed core, and a flow cell or other system for sample infusion. Antibodies are covalently bound to the surface of the core, and fluorescently labeled antigens (Ag*) are introduced into the flow cell surrounding the optical fiber. The formation of Ag* Ab complexes leads to an evanescently coupled fluorescent signal and remote detection.

Hirschfeld et al.⁸ have developed an evanescent immunosensor with a relatively large 1-mm diam

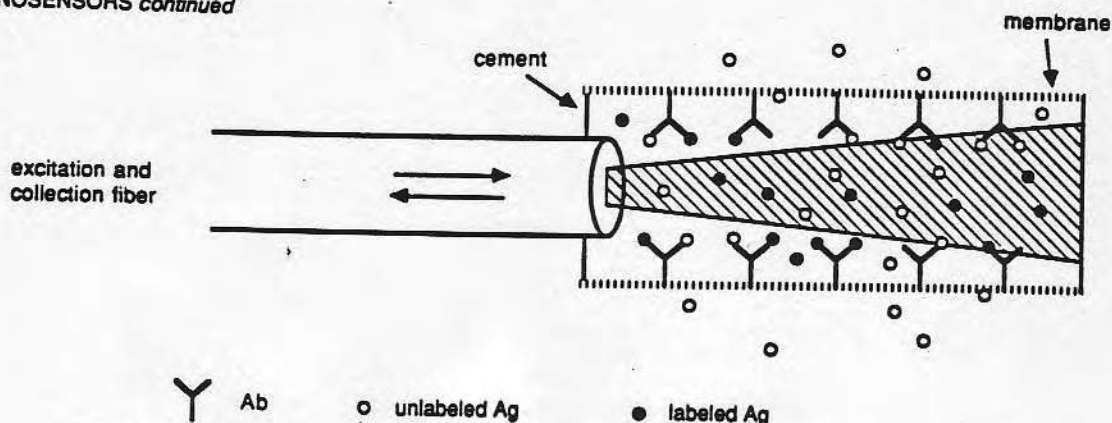


Figure 6 Schematic of an optical fiber immunosensor based on receptor-ligand exchange process.

optical rod positioned in the center of a slightly larger capillary tube. Antibodies are covalently immobilized to the sensing surface and preloaded with fluorescently labeled Ag. The liquid sample is introduced by capillary action, and a competitive assay results between the preloaded Ag* and sample Ag. Slovacek et al.⁹ performed a competitive assay with a 500- μm diam optical fiber, and detected digoxin and human ferritin antigens in solution concentrations of about 10^{-9} and $10^{-11}M$, respectively.

Sutherland et al.¹⁰ performed assays based on fluorescence, scatter, and absorption using the exposed midsection of a 600- μm diam quartz optical fiber. They observed the highest sensitivity with fluoroimmunoassay at a detection limit of about $10^{-8}M$.

Andrade and co-workers have investigated two evanescent sensor designs: a dipstick sensor using the distal end of the fiber,¹¹ and a midsection sensor.¹² Both designs used a 600- μm diam optical fiber. Experiments with these systems and similar optical designs have investigated the effect of scattered excitation light, surface-bound Ags vs bound Abs, and background fluorescence from blood serum. Considerable effort has also been devoted to regenerating the immunologically active surface for continuous monitoring.¹³

Smith et al.¹⁴ used two flat plates with antibodies bound to one plate and fluorescently labeled, partially dry antigens on the other plate. The plates were placed parallel and close to each other, and the sample solution was drawn by capillary action into the gap. A light source excited the fluors directly through the plates (in transmission mode), and the fluorescent light which evanescently coupled into the Ab-bound flat plate was collected. The evanescent coupling ensured surface sensitivity without evanescent excitation.

Conclusions

The merging of immunoassays and optical sensing can potentially be a significant benefit to clinical medicine. Research efforts have demonstrated several different designs by combining homogeneous and heterogeneous assay methods with the light transmitting and evanescent features of optical fibers. Sensitivities reported for fiber optic fluoroimmunosensors are in the 10^{-8} to $10^{-11}M$ range, which is adequate for most clinical applications. In addition, factors which have not been addressed in this article such as stability,

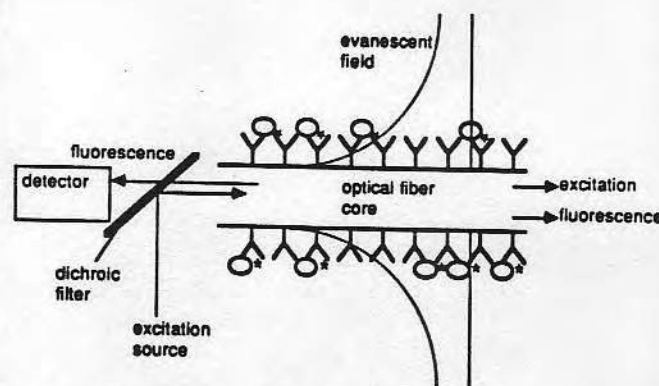


Figure 7 Schematic illustration of a fiber optic fluoroimmunosensor. This figure is a general guide, and actual systems may vary in detector placement, filter arrangement, light source, and assay method.

intrinsic fluorescent backgrounds, and biocompatibility, must be considered. These factors are being investigated, and the overall future of optical fluoroimmunosensors looks promising.

References

1. YALOW, R.S. and BERSON, S.A., *J. Clin. Invest.* 39, 1157 (1960).
2. MARCUSE, D.A., *Theory of Dielectric Optical Waveguides* (Academic Press, New York, 1972).
3. LEE, E.H. et al., *Appl. Optics* 18, 862 (1979).
4. TROMBERG, B.J. et al., *Anal. Chem.* 59, 1226 (1987).
5. ANDERSON, F.P. and MILLER, W.G., *Clin. Chem.* 34, 1417 (1988).
6. MANSOURI, S. and SCHULTZ, J.S., *BioTechnology*, Oct., 885 (1984).
7. LIU, B.L. and SCHULTZ, J.S., *IEEE Trans. on Biomed. Eng.*, BME-33, (2), 133 (1986).
8. HIRSCHFELD, T.E., U.S. Patent No. 4,447,546 (1984).
9. SLOVACEK, R. et al., *Proc. Electrochem. Soc.* 87, 456 (1987).
10. SUTHERLAND, R.M. et al., *Clin. Chem.* 30, 1533 (1984).
11. ANDRADE, J.D. et al., *IEEE Trans. Electron. Dev.* ED-32, 1175 (1985).
12. YOSHIDA, D.E. et al., *Electrochemical Society Meeting*, Chicago, Illinois, October, 1988.
13. ANDRADE, J.D. et al., *Proc. SPIE*, 718, 280 (1987).
14. BRADLEY, R.A. et al., *Phil. Trans. R. Soc. Lond.*, B316, 143 (1987).

Oxidation of Polystyrene and Pyrolytic Carbon Surfaces by Radiofrequency Glow Discharge

G. K. IWAMOTO, R. N. KING, and J. D. ANDRADE

Surface Analysis Laboratory, College of Engineering, University of Utah,
Salt Lake City, UT 84112

Plasma treatment is widely used commercially for polymer surface modification. Plasma discharge treatments are used to improve adhesiveness and printing properties, to improve cell adhesion to tissue culture substrates (1) and to etch or clean the surfaces of materials (removal of photoresist materials on semiconductors, for example (2)). The surface characterization of plasma-modified surfaces is important in order to provide greater insight into how the properties are changed.

Plasma treatment involves the production of chemically active species and ultra-violet radiation. Conventional methods of surface modification are often limited by the temperature needed for surface treatment, the leaching or toxicity of chemical agents used, and the spectral and geometric limitation of UV treatments. Plasma treatment also provides a means of selectively modifying the surface while the bulk properties remain generally unaffected (1).

In this study polystyrene and pyrolytic carbon (3) were used to investigate the nature of plasma surface modification. Polystyrene is widely used as a material for bacteriological cell culture and, in a surface-treated, oxidized form, is widely used as a solid substrate for in vitro cell culture. It is generally assumed that commercial polystyrene cell culture substrates are surface-treated by a corona or radio frequency glow discharge (RFGD) process. Although these materials are extensively used, no general surface characterization is available.

Radio frequency glow discharge (RFGD) plasmas were used in this study. Glow discharge plasmas are characterized by average electron energies of 1 to 10 eV and electron densities of 10^{12} to 10^{13} cm⁻³. Glow discharges, also called cold plasmas, are characterized by a lack of thermal equilibrium between electron temperature (T_e) and gas temperature (T_g). Typical ratios are on the order of $T_e/T_g = 10$ to 10^4 . Thus, the T_g of a glow discharge remains near ambient temperatures while the electrons are suffi-

ciently energetic to rupture bonds. This makes this type of plasma quite useful in applications involving thermally sensitive materials (4).

Surface modification by a plasma usually results in changes in surface wettability, molecular weight, and other chemical changes. Molecular weight changes occur from chain scission and crosslinking. Chemical changes occur from the addition or abstraction of groups on the surface, which in turn influence the wettability of the surface. Almost all changes produced by plasma modification are confined to the top 1 to 10 μm of the surface (1).

The reactions which occur are controlled by the pressure of gas, electric field strength, reaction chamber dimensions and the gas flow rate. The electric field strength determines the amount of energy imparted to the electrons. The gas pressure and tube dimensions affect the degree of ionization, atomic lifetimes, mean free path and gas temperatures. The gas flow will affect the rate that new reaction material can reach the solid surface (5).

X-ray photoelectron spectroscopy (XPS), scanning electron microscopy (SEM), and air/octane underwater contact angles were used to characterize the surfaces. XPS can provide both the atomic composition and chemical bonding information from approximately the top 70 \AA or less of the sample surfaces (6). Additional information may be gained from the XPS spectrum by observing the presence of satellite lines. The ejection of a core level electron from an atom changes the shielding of the nuclear charge and is felt by the outer shell electrons. This perturbation in the potential of the valence electrons is of sufficient energy that an electron can be excited to a higher energy level (shake-up) or be ejected (shake-off). For the C-1s line, satellite structure is seen up to ~ 12 eV above the major peaks; any other features would be lost in the inelastic tail which occurs ~ 15 -20 eV above the major photoionization peak. Clark's studies on polymer systems have shown that polymers must have an unsaturated backbone or unsaturated pendant groups to have observable satellite 6.6 eV above the C-1s line (7). The satellite is attributed to $\pi \rightarrow \pi^*$ transitions. Studies of alkane-styrene copolymers show that the intensity of the satellite peak is related to the number of styrene groups in the chain (8), and to the substituents on the pendant phenyl group (8).

Contact angle measurements provide information on the wettability of the sample, the surface energetics of the solid, and the interfacial properties of the solid-liquid interface. The samples were immersed in water and captive air and octane bubbles were determined by measuring the bubble dimensions. By measurement of both air and octane contact angles the surface free energy (γ) of the solid-vapor (γ_{sv}) interface may be calculated by use of Young's equation and the harmonic mean hypothesis for separation of the dispersive and polar components of the work of adhesion. This method for determination of surface and interfacial proper-

ties has been discussed in detail (9, 10). Because the measurement is made underwater, it is basically a receding angle measurement in the case of the air/water/solid measurement, thus γ_{sv} values obtained are larger than those commonly reported, which are generally advancing angle measurements (see (10) for a complete discussion).

Scanning electron microscopy was used to detect changes in surface topography due to the plasma treatment. Preferential etching of the material will change the surface topography. The formation of volatile, low molecular weight species under the surface of the material can produce bubbles (1).

Measurement of substrate surface charge was not performed in this study. A change in surface charge might be expected due to the plasma treatment either by ion implantation or by formation of ionizable functionalities on the substrate surface.

Change in contact angles as a function of storage time was also not studied. Studies on polystyrene indicate that the contact angle does change with time after plasma treatment (11).

Experimental

Samples of polystyrene were cut from Petri dishes (Falcon 1008, Falcon Plastics, Oxnard, California). Unalloyed low temperature isotropic (LTI) carbon samples were obtained from the General Atomic Company (Pyrolite - registered trademark of General Atomic Company, now Carbo-Medics, Inc.).

The polystyrene samples were used as received. Examination by XPS showed only carbon on the surface (XPS does not detect hydrogen). The pyrolytic carbon samples were prepared by a "steady state" fluidized bed process (12). The carbon samples were polished by the manufacturer using γ -alumina. Before use in this study the pyrolytic carbon samples were ultrasonically cleaned in reagent grade methanol for five minutes. Examination by XPS of both the as received and ultrasonic methanol cleaned samples showed removal of small amounts of chlorine, magnesium, silicon, and sulfur by the cleaning procedure.

The samples were oxidized using a commercial plasma discharge unit (Plasmod registered trademark of Tegal Corporation, Richmond, California), which operates at 13.56 MHz and has a variable power output from 0 to 100 watts. A variable leak valve (Granville-Phillips Company, Boulder, Colorado), a three-way valve and other modifications were added to provide a better vacuum, to control the gas flow rate and to control the gas pressure.

The samples were inserted into the RFGD unit in air and placed on the bottom-center region of the reaction chamber. In all experiments the top surface was the analysis surface. The reaction chamber was evacuated to 10^{-2} torr pressure and then backfilled with the reaction gas to above 2000 mmHg pressure and then re-evacuated. This process was repeated three times. The

gases used in this study were helium and oxygen. The helium was liquid nitrogen cold trapped during backfill to remove condensable impurities. After the third backfill and pumpdown to 10^{-2} torr pressure, the gas flow rate was adjusted to correspond to 0.4 torr pressure, which was maintained during discharge. 0.4 torr pressure was determined to give minimal deposition of silicon on the sample surface. The silicon sputtering originated from the Pyrex walls of the reaction chamber during plasma treatment. Lower pressures gave appreciable amounts of silicon deposition on the sample as determined by XPS examination. The samples were exposed to the helium gas for various amounts of time at 50 watts of power output. The samples were then exposed to a helium gas purge for various amounts of time at above 4 torr pressure and then exposed to oxygen at above 4 torr pressure for five minutes. The samples were stored in Petri dishes in air until surface characterizations were performed. It was found if the samples were exposed to air instead of oxygen after the inert gas purge that both oxygen and nitrogen functionalities were observed by XPS examination.

Oxygen plasmas were used on the pyrolytic carbon. The procedure was the same, except that the samples were exposed to an oxygen purge for 5 minutes after the discharge. XPS spectra were obtained with a Hewlett-Packard 5950 B instrument utilizing monochromatic Al $K\alpha_{1,2}$ radiation at 1487 eV. The samples were mounted in air, inserted into the spectrometer, and analyzed at ambient temperatures in a 10^{-2} torr vacuum. Power at the X-ray source was 800 watts. Instrument resolution was nominally 0.8 eV or less as measured by the full width at half maximum of the C-1s line from spectroscopic grade graphite. An electron flood gun operating at 0.3 mA and 5.0 eV supplied a flux of low energy electrons to minimize charging artifacts in the resulting spectra.

Wide scans (0 to 1000 eV) were performed for surface elemental analyses. The wide scans were carefully inspected for trace element contamination. Detailed 20 eV scans of the C-1s (275 to 295 eV), O-1s (520 -540 eV) and Al-2s (105 to 125 eV) regions for the pyrolytic carbon and of the C-1s and O-1s for the polystyrene were run to determine both elemental stoichiometry and chemical shifts. Standards were available to give accurate chemical shift data for various carbon-oxygen functional groups. These included poly(ethylene terephthalate), poly(ethylene oxide) and anthraquinone (17). The latter was run at -50°C in order to minimize volatility under our high vacuum conditions. Table I summarizes these results. All spectra were charge - referenced to a C-1s line for an alkyl-like carbon at 284.0 eV. The Scofield theoretical XPS photoelectric cross sections (13) were used for elemental quantitation.

Scanning electron micrographs were obtained on a Cambridge Mark II Stereoscan SEM. The samples were mounted on the specimen mounts with double-sided tape. Silver paint along the edge of the sample provided electrical contact between the specimen mount and

Table I

Chemical shifts in the C-1s line for poly (ethylene terephthalate), polyethylene oxide, and anthraquinone. (See also Reference 17).

Material	Observed Binding Energy (eV)*	ΔBE^{**}	Functional Group
	284.0	0.0	alkyl and/or aromatic
Polyethylene terephthalate	285.6	+1.6	ether
	288.0	+4.0	ester
	285.8	+1.8	ether
Polyethylene oxide	285.8	+1.8	ether
Anthraquinone	284.0	--	alkyl or aromatic
	286.5	+2.5	quinone

* Charge-referenced to C-1s at 284.0 eV

** Binding Energy -284.0 eV = ΔBE

the sample. The samples were coated with carbon and gold to reduce charging. The analyzing vacuum was about 10^{-4} torr.

Contact angles were determined by immersing the sample in doubly-distilled water and measuring the height and diameter of both air and octane bubbles in water (9). The bubbles were introduced on the sample surface using a microliter syringe. The height and diameter were measured by use of micrometers which manipulated a stage holding the sample immersed in water. The bubbles were observed through a microscope using a 20X long working distance objective and a 15X eye-piece equipped with a crosshair reticle. The bubble was manipulated across the crosshair and the dimensions were read directly from the micrometers. The sample box was back illuminated by a variable light source. The bubble volume was approximately 0.1 to 0.2 μl and the bubbles were applied to the surface by forming a bubble at the tip of a micro syringe and then snapping the tip to allow the bubble to float up to the water-sample interface. The bubble volume was minimized in order to avoid buoyancy effects. The octane was 99.99% pure n-octane (Aldrich Chemicals -Gold Label Octane). Temperature of the immersion bath was 26°C . Figure 1 schematically illustrates the geometry of the contact angle measurement. The contact angles were calculated using the equation

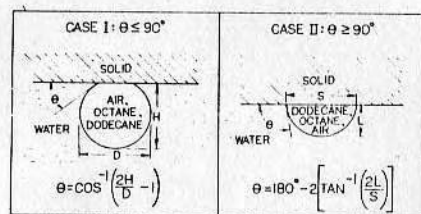


Figure 1. Schematic of both cases for contact angle calculation

$$\phi = 180 - 2 \tan^{-1} \left(\frac{2E}{S} \right) \text{ for } \phi \geq 90^\circ \text{ and } \phi = \cos^{-1} \left(\frac{2H}{D} - 1 \right) \text{ for } \phi \leq 90^\circ.$$

This technique measures the fully hydrated solid-water interface. In essence the air/water/solid angle is similar to a receding water contact angle in the conventional contact angle geometry. By probing the fully hydrated solid/water interface, the polar components of the solid surface are more optimally evaluated. As it is the solid/water interface which is of primary interest for biological interactions, we feel this method is more appropriate for surface characterization for our purposes. The use of air and octane angles also allows one to deduce the fully hydrated solid surface free energy and the solid/water interfacial free energy. Assumptions also allow the fully hydrated solid surface free energy to be decomposed into its apolar and polar components (10).

Results and Discussion

Polystyrene. Table 2 presents the carbon:oxygen ratios as determined by XPS. The as received and methanol-cleaned materials were essentially unoxidized, with carbon:oxygen ratios of the order of 100 to 1 or greater. The material which was helium plasma treated was extensively oxidized with a C:O ratio of approximately 3.5:1. The air and octane angles at the solid/water interface are also presented for those two cases. The air angle, which can be interpreted as a conventional water receding contact angle, is approximately 85° and decreases to approximately 14° on plasma treatment, indicating a substantial increase in surface wettability. The XPS spectra of the as received polystyrene show the presence of the C-1s aromatic satellite at 290.70 eV, 6.7 eV from the main carbon 1s line with approximately the correct

Table II

Carbon: Oxygen (C/O) Ratios, as determined by X-ray photoelectron spectroscopy and contact angle data for polystyrene.

Sample	C/O Ratios	Contact Angle (10)	
		Air	Octane
As received	100/1	$83 \pm 4^\circ$	$135 \pm 5^\circ$
Methanol Cleaned (Ultrasonic)	98/1	$82 \pm 4^\circ$	$135 \pm 5^\circ$
Helium Plasma	3.5/1	$14 \pm 4^\circ$	$14 \pm 4^\circ$

intensity ratio (8). The satellite peak is reduced to background level for the helium plasma treated, oxidized material, suggesting a considerable decrease in aromaticity of the polystyrene in the surface volume examined by XPS (see Figure 2). Results from helium plasma treated polystyrene are essentially identical to those found with "tissue culture" polystyrene produced by Falcon Plastics.

Scanning electron micrographs of the sample showed no gross etching of the surface. Polystyrene has no oxygen in the polymer which can form atomic oxygen in the plasma, therefore etch rates due to oxidative degradation are expected to be low. Plasma exposure times were not long enough to create low molecular weight volatile species under the surface. These can diffuse to the surface and form bubbles, as is often seen in polyethylene (1).

Hansen (14) reports a decrease in molecular weight in a helium plasma and Westerdahl (15) reports a change in contact angle to higher wettability for both helium and oxygen plasmas.

Pyrolytic Carbon. Polished LTI carbon is composed of a crystalline graphitic-like microstructure, combined with amorphous material (16). The polished samples have been shown to be oxidized with a C:O ratio of about 10:1, containing three major types of carbon-oxygen functionalities: quinone-like, ether-like, and ester-like (17).

Electrochemical studies of carbon samples have shown that both quinone-like and ester-like groups are present (18).

In this study various discharge times in oxygen and helium gas plasmas were used. The carbon/oxygen ratio varied from 7 to 1 in the as received material to 1.2 to 1 for the treated samples (see Table 3).

A rise in the amount of aluminum, as can be seen in Table 3, is also noticed after plasma treatment. The increase in aluminum at the surface may be due to preferential etching of surface carbon, uncovering Al_2O_3 , which is thought to be embedded in the polishing process. M. Millard has seen this same type of phenomena when plasma etching cells, i.e., the organic portion of the cells is etched away concentrating inorganic trace elements on the surface of the sample (19). The aluminum peak was strongest after oxygen plasma treatment, probably due to higher etching rates.

The increase in the aluminum peak is accompanied by the growth of lower binding energy oxygen and carbon peaks (see Figure 3). All three peaks were observed to move up in binding energy when the flood gun was turned off. Shifts in binding energy due to the flood gun occur when the sample is non-conducting. The flood gun is used to provide a source of low energy electrons to the sample to counter positive charging of a sample due to the electrons being ejected. The excess supply of electrons provided by the flood gun charges the sample negatively and lowers the apparent binding energies of the elements. For conducting

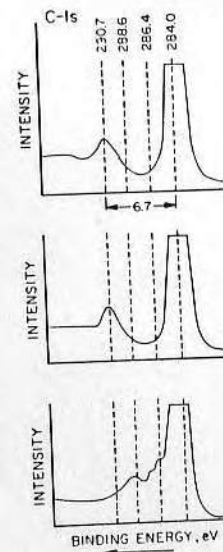


Figure 2. XPS spectra of the C-1s region of PS.

Flood gun conditions, 0.3 ma, 5 eV. The C-1s alkyl line was approximately 279.0 eV; the spectra above are charge-referenced to 284.0 eV for the alkyl carbon line. Spectrum A is the as-received material; note the presence of the aromatic satellite at 6.7 eV from the main carbon line at 284.0. Note also the absence of any carbon-oxygen functionalities as evidenced by the lack of structure between 284 and 290: (a) as-received material; (b) methanol-cleaned; (c) oxygen plasma-treated material. Note the decrease in the satellite line at 297 eV; it has disappeared to nearly background level. Also note the presence now of two carbon-oxygen functionalities as evidenced by apparent peaks at about 288.6 and 286.4 eV, characteristic of ester or carboxylic acid, and ether or hydroxyl carbon, respectively.

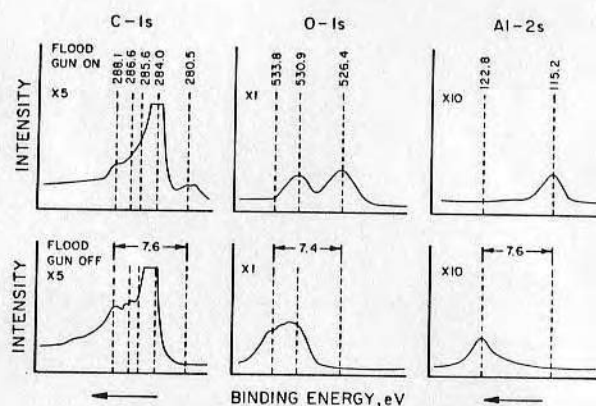


Figure 3. XPS spectra of the (a) C-1s region; (b) O-1s region, and (c) Al-2s regions of the oxygen plasma-treated pyrolytic carbon.

The upper spectra are with the electron flood gun on for charge compensation, the bottom spectra are with the electron flood gun off. Note in the upper spectrum that the main carbon peak appears at 284.0 eV, as expected for a conducting material such as pyrolytic carbon. Note also the presence of the weak apparent doublet in the vicinity of 280.5 eV. The Al-2s top far right appears at about 115.2 eV or charge shifted down stream from its apparent normal position. Comparing these upper spectra with the flood gun off spectra and looking at the relative peak positions, one can deduce (see text) that there is an insulating component in the surface region of the material that charge shifts to higher binding energies in the absence of the flood gun and is pushed to lower binding energies in the presence of the flood gun. Note also that there are a number of major lines that are not affected by the flood gun conditions. These, of course, are those intrinsic to the conductive pyrolytic carbon structure. The insulating material which is influenced significantly by the flood gun conditions is attributed to Al_2O_3 particles embedded in the carbon during the polishing process.

Table III

Carbon: Oxygen (C/O) ratio and atomic percentages as determined by X-ray photoelectron spectroscopy for pyrolytic carbon.

Treatment Type	C/O Ratios	Atomic Percent			
		C	O	Al	Trace*
As Received	8	85.5	10.4	1.4	Cl, Mg,
Methanol Cleaned (ultrasonic)	6	85	13.4	1.6	—
Helium Plasma Treatment	2-4	60-70	34-27	5-3	—
Oxygen Plasma Treatment	1.2-1.4	56	36.5	7.5	—

* Trace less than 1 atomic percent.

samples the flood gun will not affect the binding energy since the sample is in electrical contact with the grounded sample probe. Grunthaner has reported the effect of a flood gun on non-conducting samples and has used it to investigate the chemical composition of non-conducting oxides formed on metal catalyst systems (20).

In the pyrolytic carbon, aluminum, oxygen, and carbon peaks were observed to move in binding energy as a function of the flood gun conditions. Also a carbon peak and an oxygen peak remained unaffected by the flood gun (see Figure 3). The majority of the carbon and oxygen are unaffected by the flood gun and all the aluminum moves with the flood gun. From these results it is concluded that the major portion of the sample is conductive pyrolytic carbon; islands of non-conducting Al_2O_3 , with some carbon and oxygen associated with it, are being exposed on the surface due to plasma etching.

SEM of the samples shows a change in the surface roughness after glow discharge treatment. The change is due to etching of the surface by the plasma treatment and supports the noticed increase in amount of aluminum detected by XPS. Energy dispersive analysis of X-rays of the sample could not distinguish between aluminum on the surface and aluminum embedded below the surface

due to higher analysis depths. The surface appeared rougher after etching. The change in topography is probably due to preferential etching of the amorphous portion of the pyrolytic carbon.

As the samples were highly oxidized from the beginning, due to the polishing process (17), no real change in contact angle was observed.

Summary

Pyrolytic carbon and polystyrene surfaces were studied by X-ray photoelectron spectroscopy (XPS), contact angles, scanning electron microscopy (SEM), and energy dispersive analysis of X-rays (EDAX). The materials were radiofrequency glow discharged (RFGD) in helium and oxygen plasmas. RFGD of the polished carbons increased the degree of oxidation and the Al content. The increased Al content is interpreted as due to exposure of Al_2O_3 particles embedded in the polishing process. This is confirmed by flood gun-charging results.

RFGD polystyrene was oxidized, wettable, and of a decreased aromatic character as determined by analysis of XPS C-1s satellite spectra. The RFGD oxidation process etches the surface as witnessed by scanning electron micrographs.

These data are of interest in understanding the behavior of polished carbon and oxidized polystyrene in biomedical applications, including surgical implants and solid substrates for in vitro cell cultures.

Acknowledgements

Portions of this work were supported by NIH Grant #HL16921-04 and the University of Utah Faculty Research Committee.

Abstract

Surface characterization of RF plasma modified polymers is necessary in order to understand and improve certain properties including cell adhesion to tissue culture substrates. Radio frequency glow discharge (RFGD) plasmas were used to modify the surfaces of polystyrene and pyrolytic carbon. Surface characterization by X-ray photoelectron spectroscopy (XPS), scanning electron microscopy (SEM), and air and octane contact angles were performed on the as received and plasma modified samples. Plasma modification of polystyrene produced a number of carbon-oxygen functional groups and decreased both air and octane contact angles. Plasma modification of pyrolytic carbon showed an increase in aluminum and oxygen on the surface, probably due to preferential etching of surface organics, exposing the inorganic component of the sample. The aluminum and oxygen are probably from γ -alumina, used in the polishing of pyrolytic carbon. SEM also showed a change in topography indicating preferential etching.

Literature Cited

1. Hudis, M., in "Techniques and Applications of Plasma Chemistry," (J.R. Hollahan and A.T. Bell, Eds.), Chap. 3. John Wiley and Sons, New York, 1974.
2. Kirk, Ralph W., in "Techniques and Applications of Plasma Chemistry," (J.R. Hollahan and A.T. Bell, Eds.), Chap. 9. John Wiley and Sons, New York, 1974.
3. Bokros, J.D., *Carbon*, 1977, 15, 355.
4. Bell, A.T., in "Techniques and Applications of Plasma Chemistry," (J.R. Hollahan and A.T. Bell, Eds.), Chap. 1. John Wiley and Sons, New York, 1974.
5. Hollahan, J.R., *J. Chem. Ed.*, 1966, 43, A401.
6. Hall, S.M., Andrade, J.D., Ma, S.M., King, R.N., *J. Electron Spectrosc.*, 1979, 17, 181-189.
7. Clark, D.T., and Dilks, A., *J. Poly. Sci.*, 1976, 14, 533.
8. Clark, D.T., Adams, D.B., Dilks, A., Peeling, J., and Thomas, H.R., *J. Elect. Spect.*, 1976, 8, 51.
9. Andrade, J.D., King, R.N., Gregonis, D.E., Coleman, E.L., *J. Poly. Sci. Symp. C.*, 1978, 66, 313.
10. Andrade, J.D., Ma, S.M., King, R.N., Gregonis, D.E., *J. Coll. Interface Sci.*, 1979, 72, 488.
11. Triolo, P., Thesis, Department of Bioengineering, University of Utah, June, 1980.
12. Akins, R.J. and Bokros, J.C., *Carbon*, 1979, 12, 439.
13. Scofield, J.H., *J. Electron Spect.*, 1976, 8, 129.
14. Hansen, R.H., Pascale, J.V., DeBenedictus, T., and Rentzepis, P.M., *J. Poly. Sci.*, 1965, A3, 2205.
15. Westerdahl, C.A.L., Hall, J.R., Schramm, E.C., and Levi, D.W., *J. Colloid Interface Sci.*, 1974, 47, 610.
16. Biscoe, J., and Warren, B.E., *J. Appl. Phys.*, 1942, 13, 364.
17. King, R.N., Andrade, J.D., Haubold, A.D., and Shim, H.,

"Surface Analysis of Silicon-Alloyed and Unalloyed LTI Pyrolytic Carbon," in this volume.

18. Evans, R. and Kuwana, T., Anal. Chem., 1977, 49, 1632.
19. Millard, M.M., "Surface Characterization of Biological Materials by X-ray Photoelectron Spectroscopy," in D.M. Hercules, et al., Eds., Cont. Topics in Anal. and Clin. Chem., 1978, 3, 1.
20. Grunthaner, F., Ph.D. Dissertation, California Institute of Technology, 1974.

RECEIVED March 23, 1981.

Insulin Adsorption: Intrinsic Tyrosine Interfacial Fluorescence

Insulin adsorption at a solid-liquid interface was studied using a new technique, total internal reflection fluorescence (TIRF). TIRF has been used both to study the adsorption of proteins labeled with an extrinsic fluor, such as fluorescein isothiocyanate (1-3), and unlabeled proteins containing tryptophan (4).

The adsorption and macroaggregation of insulin is a serious problem in many insulin preparations, particularly in delivery devices which require small volumes and therefore high insulin concentrations (5). A study of insulin adsorption is of interest in improving such devices and in optimizing the stability of insulin solutions for the treatment of diabetes (6).

Interfacial fluorescence allows one to perform real time, *in situ* measurements of protein adsorption. An evanescent wave is produced when light of wavelength, λ , traveling through a dense medium of refractive index, n_1 , encounters a second medium with a lower refractive index, n_2 . Total internal reflection occurs if the angle of incidence, θ , is greater than a critical angle, θ_c . The critical angle is defined by the equation: $\theta_c = \sin^{-1}(n_2/n_1)$. Under such total reflection conditions, the evanescent wave penetrates into the second medium. The amplitude falls off exponentially with distance into the rarer medium as a function of the wavelength of the incident light, the angle of incidence, and the refractive index ratio, n_2/n_1 (7). The depth of penetration for a quartz-water ($n_1 = 1.33$)/($n_2 = 1.47$) interface using UV light ($\lambda = 2800$ Å) is approximately 1000 Å, thus only those proteins within about 1000 Å of the interface are excited. Therefore, TIRF has the sensitivity to monitor protein adsorption. Because of the exponential decay of the signal into the low refractive index phase, the method detects adsorbed proteins with much more sensitivity than proteins in the bulk solution (4).

Interfacial fluorescence has been used to study the adsorption of fluorescently labeled proteins (1-3) and proteins containing tryptophan (4). A study of the fluorescence of tyrosine intrinsic to proteins offers a variety of problems which must be considered. The fluorescence yield of tyrosine is 10 times lower than tryptophan (8). This is in part due to energy transfer if both tryptophan and tyrosine are present in the molecule. Tyrosine can transfer its energy to tryptophan in a nonradiative manner (9); consequently, the tryptophan will exhibit the fluorescence. The fluorescence of tyrosine, when incorporated into a

protein, is also quenched by the peptide bond. Various species in the solution, such as phosphate, amines, and carbonyls, can cause quenching of tyrosine. The fluorescence yield of tyrosine is dependent on temperature; the yield increasing as temperature is decreased. The fluorescence of tyrosine is dependent on the ionization state of the phenolic hydroxyl group, therefore, the fluorescence is dependent on the pH and on the type of bonding in which the tyrosine residue is involved in the protein. Eight classifications have been used to describe tyrosine fluorescence in proteins (10).

The structure of insulin has been extensively studied. Crystal structure and amino acid sequence have been well defined. Insulin is a small protein (molecular weight 5750) and is believed to have a similar solution and crystalline state structure as determined via X-ray diffraction studies. However, very recent work (11) suggests that native monomeric insulin is structurally different than the dimer and hexamer forms which have been extensively studied in the literature. The importance of zinc in the crystal is well known; aggregation may depend on the amount of Zn present as well as on other variables (6).

Insulin exists in solution in monomer, dimer, hexamer, and larger aggregates. The two zinc dimer and hexamer forms have been well characterized (12-14). The concentrations of the various insulin forms have been shown to be dependent on the total concentration of insulin in solution. Insulin aggregates have been studied by ultracentrifugation at pH 2 (15) and pH 7 (16).

The monomer form of insulin has two hydrophobic strips on its surface. The hydrophobic strips are important in dimer formation and possibly in the insulin-insulin receptor interaction. This has been studied by substituting various hydrophobic strip amino acid residues and measuring the resultant insulin activity (10, 17-19). A second hydrophobic strip on the monomer surface is exposed on both sides of the dimer, allowing three dimers to hydrophobically interact to form the hexamer with the zinc in the middle (12).

Insulin contains four tyrosine residues. The two at positions A14 and A19 are buried in the hydrophobic core and are H-bonded to carbonyls and consequently produce no fluorescence. The tyrosines may also be quenched due to the proximity of disulfide bonds. The reported bulk fluorescence for insulin is

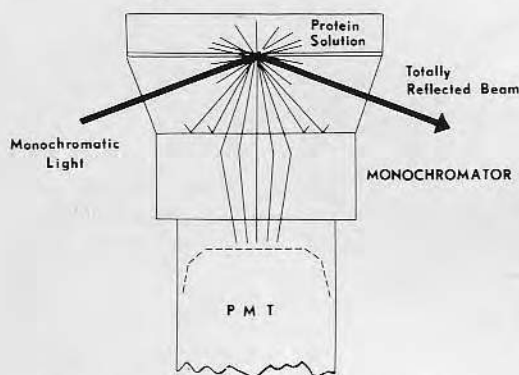


FIG. 1. Principle of total internal reflection fluorescence. Incident light (276 nm) enters a quartz dovetail prism and excites interfacial fluorescence during total reflection. The emission monochromator passed fluorescence at 305 nm. A photomultiplier tube quantitated the fluorescence photons.

0.18 that of free tyrosine. The loss of fluorescence is due to the above mentioned problems and also to fluorescence quenching from the peptide bond (10). Other factors such as temperature, ions in solution, ionization state, and conformation may cause fluorescence quenching.

As insulin has a fluorescence temperature coefficient of $-1.0\%/^{\circ}\text{K}$, all experiments were run at 25°C to maximize fluorescence yield. Phosphate ions, amines, or high concentration of COO^- can cause quenching of tyrosine. Consequently, these studies were conducted in 0.1 N NaCl , pH 7.0–7.5. Molecular oxygen does not quench tyrosine as it does tryptophan so the solutions were not deaerated before each run (9). Insulin in strongly basic (pH > 9) solutions loses fluorescence due to ionization of the phenolic groups. All experiments reported here were run at pH 7–7.5.

Porcine insulin solutions were obtained from Novo (Wilton, CT 06897) as Actrapid U-80 and U-200, Lot #521*9, Batch 680 with glycerin and methyl paraben additives. Tyrosine was obtained from Sigma. Poly(dimethyl siloxane) (PDMS) was a gift from Avco Medical Products and prepared as a 1% by volume solution in chloroform.

Insulin was isolated from the source by separating the preservatives on a G-25 Sephadex column. The separation was necessary since both preservatives used, phenol and parahydroxy benzoate, had UV absorption and fluorescence which compromised the TIRF signal.

Electrophoresis was run on 20% crosslinked polyacrylamide gels in 25 mM Tris buffer for approxi-

mately 4 hr using an Ortec pulsed power system. Transmission fluorescence spectra were obtained on an Aminco-Bowman spectrofluorometer (American Instruments Corp., Model 4-8202) scanning emission spectra from 200 to 800 nm with an excitation wavelength of 276 nm. UV absorption was measured on a Cary-15 spectrophotometer from 200 to 350 nm using a 1-cm cell. Such spectra were used to check for impurities as well as to determine the absorption maximum in order to select the best excitation frequency for both transmission fluorescence and TIRF. Absorbance was also used to determine the concentration of tyrosine and insulin using 1.4×10^3 (8, 20) and $0.553 \times 10^5\text{ mole}^{-1}\text{ dm}^{-1}$, respectively, for the molar extinction coefficient. A Jasco model 4-40 was used to perform circular dichroism measurements.

Circular dichroism showed bands at 276 and 235 nm. Scans did not go below 230 nm due to H_2O absorption for the conditions used. Transmission fluorescence gave a strong emission band at the expected wavelength for tyrosine. This was confirmed in the TIRF spectra. UV absorption spectra were obtained for every separation performed as a check on the separation procedure and to determine maximum absorption for determination of insulin concentration.

Adsorption was measured at a hydrophilic, fused quartz prism surface and a coated quartz surface prepared by evaporating 1% (v/v) poly(dimethyl siloxane) (PDMS) in chloroform on the quartz prism. This is a room temperature vulcanizing (RTV) formulation which crosslinks the rubber at room temperature. The PDMS coating thickness was less than 500 Å and well within the evanescent wave penetration depth. The quartz prism was mounted in a holder with a flow cell made up of the prism, a silicone rubber gasket, and a black anodized aluminum block which had channels to provide for flow. The priming volume was approximately 5 ml. A high pressure Hg/Xe lamp was used as a source of UV light. The excitation wavelength was selected by use of a monochromator (Jobin Yvon H-10). The monochromatic light ($\lambda = 276\text{ nm}$) was then focused onto a mirror which in turn reflected the light into a quartz dovetail prism with 70° faces. Total internal reflection occurred at the quartz–aqueous buffer interface (see Fig. 1). The evanescent wave, described above, excited proteins near the surface.

Fluorescence produced by the UV-excited proteins was measured normal to the interface (see Fig. 1). The fluorescence passed through the quartz prism and cell holder which secured the quartz prism and flow cell. The holder was attached to an emission monochromator which selected the wavelength of emitted light which was then measured by a photomultiplier tube. Photomultiplier signal output

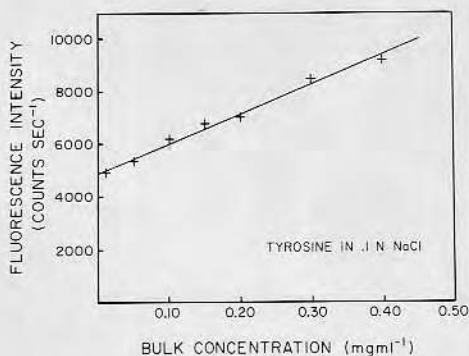


FIG. 2. Fluorescence signal intensity as a function of tyrosine bulk concentration (mg ml^{-1}) in 0.1 N NaCl . Excitation wavelength was 276 nm ; fluorescence was collected at 305 nm . The count rate increases linearly with tyrosine concentration to 0.4 mg ml^{-1} .

was fed to a preamp (Ortec 9301) and then to an amplifier discriminator (Ortec 9302). The signal was then counted by a photon counting system (Ortec 9315) and displayed digitally (Ortec 9320). The digital output was also converted to an analog signal by a D to A converter (Ortec 9325) and recorded using a strip chart recorder (Pharmacia 481) (see Ref. (4) for more details).

The flow cell and prism were cleaned before each run by first washing in detergent (Microclean) and then, after a thorough rinse in distilled water, passed through a series of four filtered, distilled water and two filtered ethanol baths with a final vapor degreasing in a Freon TES-ethanol azeotrope vapor to remove particulates which would scatter light. All cleaning steps were performed in a laminar flow-filtered air bench in a clean room. In addition, the quartz prism was further cleaned after the detergent step in chromic acid cleaning solution. Following Freon treatment, the prism was radiofrequency glow discharged in an oxygen gas plasma at $200\text{ }\mu\text{m Hg}$ and 30 W for 2 min (Plasmod, Tegal Corporation).

The flow cell and prism were mounted and aligned with the optics. A water bath recirculator was used to maintain constant temperature (Lauda-Brinkman). An excitation wavelength of 276 nm with 2-mm slits was chosen with the monochromator. The emission wavelength was at 305 nm with a 2-mm slit. Emission spectra were also obtained in the range $300\text{--}400\text{ nm}$. Experiments were run by first flushing the flow cell with 0.1 N NaCl and then establishing a baseline for approximately 1 hr . Counts were recorded. The insulin was injected and allowed to adsorb for about 1 hr , then flushed out with 60 ml of 0.1 N NaCl . Fluores-

cence signal intensity was followed as a function of time to determine the desorption characteristics.

Tyrosine solutions in 0.1 N NaCl , $\text{pH } 7.0$ were first characterized by UV absorption and transmission fluorescence spectroscopy. A value of $1.4 \times 10^3\text{ mole}^{-1}\text{ dm}^{-1}$ was used for the molar extinction coefficient; calculated bulk solution concentrations agreed well with known concentrations of prepared stock solutions. Emission spectra of buffer and tyrosine solutions were run to check emission maximum resulting in a value of 305 nm for the emission wavelength used in the rest of the experiments. A concentration range of $0.01\text{--}0.4\text{ mg ml}^{-1}$ was studied by the TIRF technique with counts taken at each concentration and after the buffer flush following each bulk concentration. Flush values remained constant, independent of concentration, indicating very little, if any, adsorption of tyrosine. The plot of fluorescence signal count rate versus bulk tyrosine concentration was linear throughout the concentration range (Fig. 2) which was limited by the solubility of tyrosine in the solution. The background count rate was due to excitation light scattered by the buffer solution. Bulk tyrosine TIRF experiments were also performed with emission slits of 0.5 to 2 mm ; all the results gave a linear slope. A wider slit allows more fluorescence to be measured with a loss in the resolution in emission wavelength. The larger slits increased the detectability for insulin.

A set of TIRF adsorption experiments were run using Novo Actrapid U-200 insulin. The initial run was on a hydrophobic surface and the insulin concentration was 0.016 mg ml^{-1} . Some adsorption could be detected by the TIRF method. Another set of runs on both hydrophilic and hydrophobic surfaces using a bulk insulin concentration of 0.33 mg ml^{-1} with identical flow rates, temperature, etc., showed no detectable adsorption onto the hydrophilic surface but a significant level of adsorption (or interfacial aggregation) at the hydrophobic surface (see Fig. 3).

Transformation of the fluorescence data into grams adsorbed protein (unit area^{-1}) requires several assumptions and involves using the bulk protein component of the TIRF signal as an internal calibration (4). Unfortunately, the bulk signal is difficult to detect for insulin unless one goes to high solution concentrations, due to the very low quantum yields for tyrosine in insulin. A more intense UV source and more optimum optics should permit detection of the bulk signal and, thereby, quantitation of interfacial insulin. Such experiments are now in progress.

The use of total internal reflection UV fluorescence to measure adsorption of insulin via intrinsic tyrosine fluorescence has been demonstrated. Tyrosine as a free amino acid exhibited a linear dependence with con-

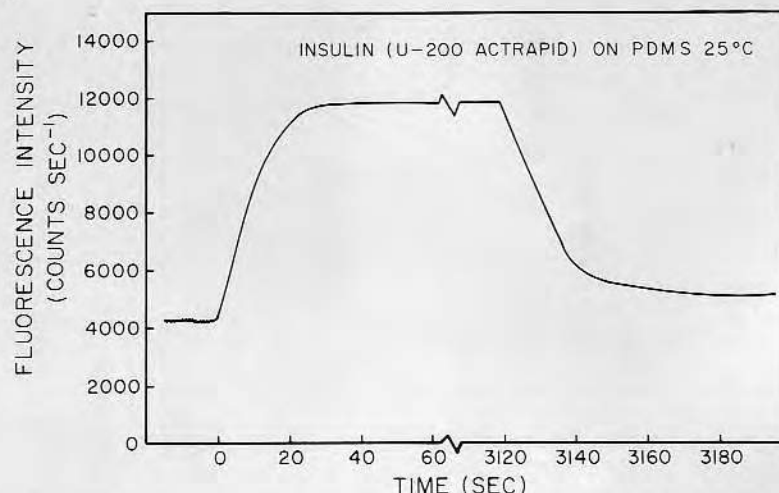


FIG. 3. Adsorption of Actrapid U-200 insulin (0.7 ml of U-200 in 10 ml of 0.1 N NaCl) onto hydrophobic quartz (quartz coated with a thin film of PDMS). Excitation wavelength, 276 nm. Emission wavelength, 305 nm. Temperature, 25°C. Background counts are due to scattered light not fully rejected by the monochromator. Time 0 represents the injection of insulin solution. The signal rapidly increases to a plateau of nearly 12,000 counts/sec within 40 sec. At 3120 sec insulin-free buffer solution was injected, resulting in rapid desorption for 20 sec followed by a slower desorption rate in another 30 or more sec. Note that some insulin is "irreversibly" bound, as the count rate after desorption (5000 counts/sec) is significantly higher than that prior to adsorption (4000 counts/sec).

centration; no detectable adsorption occurred. Insulin adsorption occurs more on hydrophobic polydimethyl siloxane surfaces than on hydrophilic quartz surfaces. High adsorption on hydrophobic surfaces may be significant with respect to insulin loss onto containers and for insulin aggregation and loss in delivery devices.

ACKNOWLEDGMENTS

We thank Novo and Avco Medical for donations of materials. G. K. Iwamoto thanks the University of Utah College of Medicine for a summer research fellowship. We also thank D. A. Wilson, University of Utah Department of Internal Medicine, for several discussions. Portions of this work were supported by NIH Grant HL 18519-05.

REFERENCES

1. Watkins, R. W., and Robertson, C. R., *J. Biomed. Mater. Res.* **11**, 915 (1977).
2. Harrick, N. V., and Loeb, G. I., *Anal. Chem.* **45**, 687 (1973).
3. Zdasiuk, B. J., M.S. Thesis, Department of Bioengineering, University of Utah, 1980.
4. Van Wagenen, R. A., Rockhold, S., Andrade, J. D., in "Morphology, Structure, and Interactions of Biomaterials" (S. L. Cooper, A. S. Hoffman, N. A. Peppas, and B. D. Ratner, Eds.), Amer. Chem. Soc., Washington D. C., in press, 1981.
5. Albisser, A. M., Loughheed, W., Perlman, K., and Bahoric, A., *Diabetes* **29**, 241 (1980).
6. Quinn, R., and Andrade, J. D., submitted for publication.
7. Harrick, N. J., "Internal Reflection Spectroscopy." Wiley Interscience, New York, 1967.
8. Freifelder, D., "Physical Biochemistry." Freeman, San Francisco, 1976.
9. Guilbault, G. G., "Practical Fluorescence." Dekker, New York, 1973.
10. Cowgill, R. W., in "Biochemical Fluorescence" (R. F. Chen and H. Edelhoch, Eds.), Chapter 9. Dekker, New York, 1976.
11. Pocker, Y., and Biswas, S. B., *Biochemistry* **19**, 5043 (1980).
12. Blundell, T., Dodson, G., Hodgkin, D., and Mercola, D., *Adv. Protein Chem.* **26**, 279 (1972).
13. Blundell, T., Dodson, G., Dodsonand, G., and Vijayon, M., *Contemp. Phys.* **12**, 209 (1971).
14. Yeung, C., Louleard, M. L., and Yip, C. C., *J. Biol. Chem.* **254**, 9453 (1979).
15. Jeffrey, P. D., and Coates, J. H., *Biochemistry* **5**, 3820 (1966).
16. Pekar, H., and Frank, B. H., *Biochemistry* **11**, 4013 (1972).

17. Katsoyannis, P. G., in "Advances in Experimental Medicine and Biology" (R. A. Comevini and D. B. Hanover, Eds.), Vol. 119. Plenum Press, New York, 1979.
18. Fredericq, E., *Arch. Biochem. Biophys.* **65**, 218 (1956).
19. Hodgkin, D., in "Diabetes," (J. S. Bajaj, Ed.), p. 155. Excerpta Medica, Amsterdam, 1977.
20. "CRC Handbook of Biochemistry and Molecular Biophysics" (G. D. Fasman, Ed.), 3rd ed. Chem. Rubber Pub. Co., Cleveland, 1976.

G. K. IWAMOTO
R. A. VAN WAGENEN
J. D. ANDRADE¹

*Department of Bioengineering
College of Engineering
University of Utah
Salt Lake City, Utah 84112*

Received June 9, 1981; accepted August 15, 1981

¹ To whom requests for reprints should be addressed.

Fibronectin Adsorption Detected by Interfacial Fluorescence

G. K. IWAMOTO, L. C. WINTERTON, R. S. STOKER, R. A. VAN WAGENEN,
J. D. ANDRADE,* AND D. F. MOSHER†

Department of Bioengineering, University of Utah, Salt Lake City, Utah 84112, and †Department of Medicine,
University of Wisconsin Medical School, Madison, Wisconsin 53706

Received November 28, 1983; accepted December 17, 1984

An interface optical technique, total internal reflection fluorescence (TIRF), permits the intrinsic tryptophan fluorescence of adsorbed proteins to be monitored continuously, *in situ*. The protein fluorescence emission spectrum provides information on the local tryptophan microenvironment, which can be related to the orientation and conformation of the adsorbed macromolecule. This technique has been applied to the adsorption of human plasma fibronectin on hydrophilic and hydrophobic amorphous silica surfaces. Our experiments using the TIRF technique have shown increased fibronectin binding and more rapid adsorption kinetics on hydrophobic silanized-silica in contrast to hydrophilic silica. Adsorption was essentially irreversible on both the hydrophilic and the hydrophobic surface. A 5-nm red shift in the fluorescence emission maximum occurred on the hydrophobic surface suggesting a change in protein conformation and/or microenvironment. Such behavior may correlate with changes in biological function noted by other workers. We have demonstrated that the *in situ* TIRF technique, utilizing intrinsic tryptophan fluorescence, is useful for probing microenvironmental effects and possibly orientation or conformational changes in adsorbed proteins. This is the first report of intrinsic TIRF fluorescence spectral changes upon adsorption.

© 1985 Academic Press, Inc.

INTRODUCTION

Fibronectins comprise a class of high-molecular-weight glycoproteins widely distributed in blood, connective tissues, and associated with cells and basement membranes. Fibronectins are involved in cell adhesion, wound healing, opsonic activity, platelet adherence, complement activation, and coagulation system activation (1).

The amino acid composition of fibronectin is not unusual; however, the tryptophan and cystine content of both Type 1 and 2 homology regions (2) is quite high (3).

Circular dichroism (CD) studies of plasma fibronectin show a pattern characteristic of tryptophan residues in differing environments as well as contributions from tyrosine and phenylalanine (4). The CD spectra show very little or no α -helical content (3-7) and 30-

35% antiparallel β structure which is resistant to both heat and intrachain disulfide bond reduction (3, 6). Intrachain disulfide bonds play a major stabilizing role in fibronectin's structural integrity (4).

The structure of fibronectin is adequately described elsewhere (3-11).

Fibronectin normally exists as a compact molecule which may be disrupted by an environmental change, adsorption, or via binding of collagen or heparin leading to a much more extended shape (4, 10, 11).

Because plasma fibronectin seems to play a role in cellular adhesion and functions to activate the coagulation system, many studies have been directed towards the study of its surface adsorption properties (12-19). A variety of surfaces have been evaluated, and in many instances the fibronectin was isotopically labeled. Grinnell has pointed out that ^{125}I -fibronectin has altered biological activity while the tritiated molecule prepared via

* To whom correspondence should be addressed.

reductive methylation retains its biological activity (13). Fibronectin is apparently very sensitive both to alterations induced by partition at the air-water interface as well as fluid shear stresses (16). It would be of great benefit then to study native fibronectin adsorption without altering it or inducing unwanted effects. Here we study the adsorption of native fibronectin in just such an environment.

METHODS AND MATERIALS

Fibronectin (Fn) was supplied frozen in 1-ml aliquots in concentrations ranging from 1 to 17 mg/ml. The material was purified and characterized by the methods of Mosher (20). The protein was "thawed" from storage at -80°C in a water bath at 37°C . The protein was then centrifuged and solution decanted to remove aggregates. The protein was then diluted using either Tris or PBS buffers at pH 7.2–7.4. Absolute concentrations were determined by UV absorption using an extinction coefficient of $\epsilon_{1\text{ cm}}^{280\text{ nm}} = 1.28$.

Total internal reflection fluorescence (TIRF) is an optical technique for monitoring protein adsorption based upon interfacial fluorescence from extrinsic fluor probes bound to the protein (23) or intrinsic fluorescence of tryptophan or tyrosine moieties integral to the protein itself (21, 22). Since the tryptophan content of fibronectin is high and situated in biologically significant domains, TIRF studies of the intrinsic tryptophan fluorescence of fibronectin may reveal conformational information of adsorbed fibronectin. The experimental configuration (21), application to protein adsorption (21–23) and quantitation (22) have been described elsewhere.

The intrinsic TIRF approach provides for continuous monitoring of interfacial fluorescence as a function of time during protein adsorption and desorption without having to compromise the protein by attaching a fluorescent probe. The fluorescence signal remaining after desorption is attributed to

bound protein (21–24). The signal intensity can be related to the amount of protein bound by the use of suitable standards and several key assumptions (22, 24).

In the static adsorption experiments the TIRF flow cell (21, 24) was initially primed with Tris (pH 7.2) buffer. Five ml of protein sample solution were injected into the flow cell with care exercised to avoid bubbles. The injection flow rate of 13 ml/min corresponded to a shear rate of $\gamma = 210\text{ s}^{-1}$. Adsorption was monitored for 40 min at $\lambda_{\text{excitation}}$ of 280 nm and $\lambda_{\text{emission}}$ of 330 nm. Desorption was monitored following a rapid flush with Tris buffer (60 ml at 60 ml/min, and $\gamma = 970\text{ s}^{-1}$) to remove bulk Fn. This rapid flush was repeated every 15 min for 45 min with continuous monitoring. Interfacial fluorescence emission spectra were obtained before adsorption, in the primed cell after adsorption, and after each 60-ml buffer flush. All spectra were obtained using $\lambda_{\text{excitation}}$ of 280 nm and $\lambda_{\text{emission}}$ was continuously monitored from 270 to 400 nm. Fn solution concentrations for the static adsorption experiments were 0.02, 0.04, and 0.43 mg/ml.

Adsorption under flow conditions was studied in PBS buffer (pH 7.4). The cell was primed with buffer and sample solutions were injected at 1 ml/min ($\gamma = 16\text{ s}^{-1}$) for 30 min using a syringe pump. Desorption was studied under two sets of conditions: (1) buffer flush at $\gamma = 210\text{ s}^{-1}$ for 2 min followed by buffer flush at $\gamma = 16\text{ s}^{-1}$ for 30–40 minutes; and (2) buffer flush at $\gamma = 16\text{ s}^{-1}$ for 40–50 minutes. Fluorescence emission spectra were taken after flow cell priming, after adsorption, after rapid flush, and after slow flush, using previously described conditions. Fn concentrations were 0.3 and 1 mg/ml.

Raw fluorescence emission spectra are continuous curves of fluorescence intensity in counts per second (CPS) as a function of wavelength at constant excitation wavelength. The instrument response or throughput correction function was experimentally determined using a secondary standard, calibrated

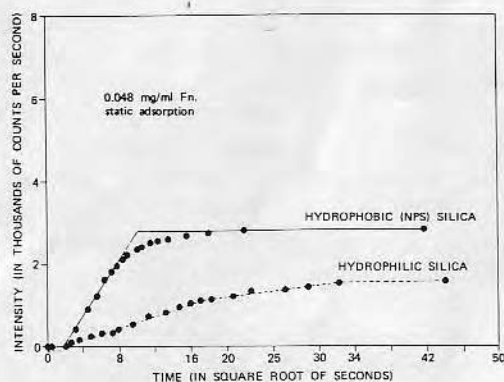


FIG. 1. Fibronectin adsorption onto hydrophilic silica and hydrophobic NPS-silica under static nonflow conditions.

light source (Optronics 245A). Emission spectra were manually corrected in 5-nm increments and in 2.5-nm increments near and through the peak maximum following background spectral subtraction.

All glass and silica slides were cleaned (21) in a low particulate environment and then radio frequency glow discharge treated. The cleaning process produced a hydrophilic silica surface, with water contact angles approaching zero degrees, as determined by the Wilhelmy plate technique (25). Hydrophobic surfaces were derived from hydrophilic silica by vapor-phase silanization (26) using *n*-pentyltriethoxysilane (NPS) (Petrarch Systems Inc., Levittown, Penn.), yielding a hydrophobic surface with receding and advancing water contact angles of 58 and 76°, respectively. Surface chemical composition was monitored by X-ray photoelectron spectroscopy (XPS).

RESULTS AND DISCUSSION

Figures 1 and 2 show rate curves that are attributed to Fn adsorbing onto the hydrophilic and hydrophobic silica surfaces, under static and flow conditions. Using an internal fluorescence signal model approach (22), the fluorescent counts were transformed into concentrations of adsorbed Fn. At binding equilibrium (plateau), hydrophobic NPS-silica

adsorbed $0.19 \mu\text{g}/\text{cm}^2$ of Fn while hydrophilic silica adsorbed $0.14 \mu\text{g}/\text{cm}^2$ of Fn, assuming a 20-nm thickness for the adsorbed protein layer (22) at the shear stress of 16 s^{-1} . The amount adsorbed is comparable to that reported by others (13, 16, 17). An increased amount of adsorbed Fn on hydrophobic surfaces has also been noted by Grinnell (13) and Jönsson (16).

A comparison of the kinetics on hydrophilic silica and hydrophobic NPS-silica indicate very different rates of adsorption in both sets of experiments. The differences are particularly pronounced in the static adsorption case (Fig. 1). The rate differences between the static and flow experiments may reflect the effect of interfacial shear stress and mass transport. As the bulk Fn concentration was low in the static adsorption case, there is a high likelihood that adsorption resulted in significant bulk solution depletion and thus the lagging kinetic curves. Since the flow cell surface area and volume were 28 and 1.4 cm^3 , respectively, the amount of Fn depleted from solution would be about $6 \mu\text{g}$ or about 9% of the total protein ($67 \mu\text{g}$) in the flow cell. This may account for the fact that equilibrium adsorption in the nonflow case was quite different for hydrophilic versus hydrophobic surfaces while in the flow case the equilibrium adsorbed Fn levels were sim-

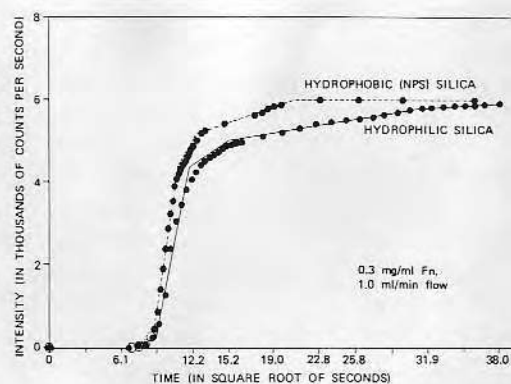


FIG. 2. Fibronectin adsorption onto hydrophilic silica and hydrophobic NPS-silica at a shear rate of 16 s^{-1} and protein solution concentration of $0.3 \text{ mg}/\text{ml}$.

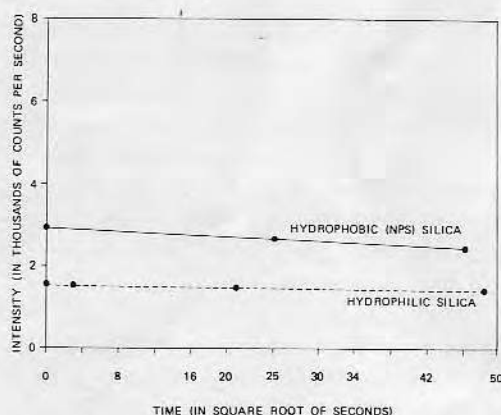


FIG. 3. Fibronectin desorption after static adsorption onto hydrophilic silica and hydrophobic NPS-silica. Both were preceded by a rapid buffer flush to remove bulk protein. Desorption is a continuation of Fig. 1.

ilar. The overall maximum amount of protein adsorbed in the flow case would result in a solution depletion no greater than 1%.

The initial rates are rapid, particularly on the hydrophobic NPS-silica, and seem to be linear in $t^{1/2}$, suggesting diffusion control up to approximately 3 min. Apparently, the first Fn molecules adsorb on contact with the hydrophobic surface. The adsorption rate on hydrophilic silica is lower and may reflect a lower protein sticking coefficient; at equilibrium the amounts adsorbed are almost equal for the continuous flow experiments of Fig. 2. The signal in Fig. 2 has several temporally separable components: (1) bulk Fn enters the flow cell ($7 \text{ s}^{1/2}$) and fluoresces due to excitation of the bulk solution by stray scattered light (22) ($7-9 \text{ s}^{1/2}$); (2) Fn diffuses into the interfacial region probed by the evanescent wave and fluoresces ($9-11 \text{ s}^{1/2}$); (3) Fn begins to adsorb on the surface until equilibrium is attained after approximately 7.5 min on NPS-silica and 30 min on hydrophilic silica. Now the fluorescence is dominated by the adsorbed species. The third time domain lasts about 5.5 and 28 min for hydrophobic NPS-silica and hydrophilic silica, respectively. There are at least two different adsorption rates observable for both surfaces.

Figures 3 and 4 illustrate the corresponding desorption for the static and flow adsorption conditions, respectively. The desorption rate and total extent of desorption was low for both the hydrophilic and hydrophobic surfaces. The data of Fig. 3 were obtained after a thorough Tris buffer flush. Both surfaces exhibited a single rate of desorption. Over a 35-min period the hydrophilic silica surface lost about 6% of the adsorbed protein signal while the hydrophobic NPS-silica surface lost 15% of the adsorbed protein signal.

The desorption curves of Fig. 4 show three time domains for Fn desorption from hydrophobic NPS-silica. Domain f^*-g^* (1 min) represents the bulk solution protein flushed from the flow cell at 16 s^{-1} . Fluorescence decreases as the bulk protein in the evanescent volume is removed. Domain g^*-h^* (5 min) represents Fn diffusion from the boundary layer into the bulk fluid and out of the evanescent volume. Domain $h^*-50 \text{ s}^{1/2}$ (36 min) represents true Fn desorption and subsequent diffusion out of the boundary layer. This last time period corresponds to that depicted in Fig. 3. As before there are single desorption rates from both surfaces; however, in the case of Fig. 4, hydrophobic NPS-silica lost about 12% of the adsorbed protein signal

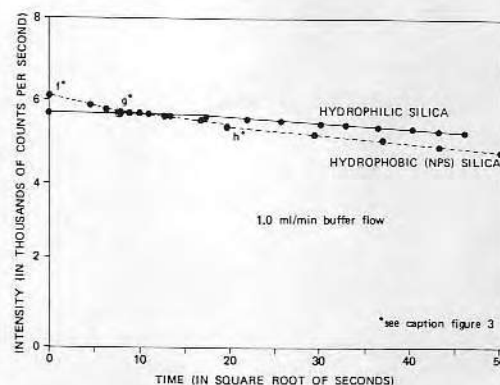


FIG. 4. Fibronectin desorption from hydrophilic silica and hydrophobic NPS-silica under flow shear conditions of 16 s^{-1} . The hydrophilic silica desorption was preceded by a 60-ml rapid buffer flush to remove bulk protein. Desorption is a continuation of Fig. 2. (*) indicates monitoring of fluorescence emission spectrum.)

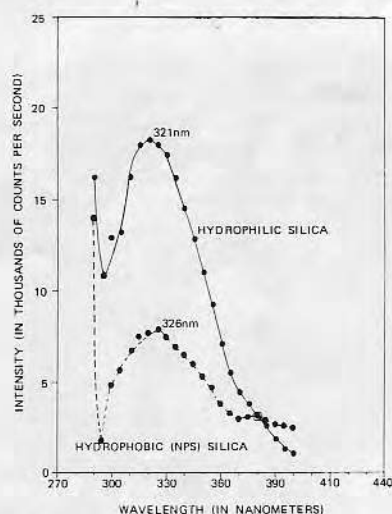


FIG. 5. Intrinsic TIRF emission spectra of fibronectin adsorbed onto hydrophilic silica and hydrophobic NPS-silica.

which is close to that observed in Fig. 3. Desorption of Fn from hydrophilic silica shows a single linear rate. The flush corresponding to f^* through h^* was not monitored. The fluorescent signal loss indicates that about 8% of the adsorbed protein is lost over the same 36-min time period ($19-50 \text{ s}^{1/2}$). This value is very close to the 6% decline for the static adsorption experiment (Fig. 3).

The fluorescence emission spectra of adsorbed Fn showed a maximum at 321 nm for protein adsorbed on hydrophilic silica and 326 nm for protein adsorbed on hydrophobic NPS-silica (Fig. 5). The bulk fluorescence spectra of fibronectin in PBS buffer showed a fluorescein maximum of 321 nm. The addition of 8 M urea, which unfolds the protein, red-shifted the emission maximum to 330 nm while the addition of 3 M guanidine chloride, which denatures the protein entirely, red-shifted the emission maximum to 350 nm, which is observed for free tryptophan in aqueous buffer. Alexander *et al.* (15) have shown Fn conformational changes with addition of 6 M guanidine chloride using fluorescence polarization and circular dichroism analyses. The fluorescence maximum 5-

nm red shift observed with Fn adsorption onto hydrophobic NPS-silica surfaces suggests that the tryptophans are in a more hydrophilic environment as a result of adsorption, moving toward the value of free tryptophan in aqueous buffer. This could occur if the protein experienced a change in conformation in the adsorbed state, resulting in some tryptophans being shifted into a more hydrophilic environment in contrast to their microenvironment in bulk solution or on hydrophilic silica. A change in conformation has been suggested by Grinnell (13) and Jönsson (16) who have noted a difference in fibronectin antibody binding to adsorbed fibronectin on hydrophobic compared to hydrophilic surfaces. Grinnell has also noted a decrease in cell interactions with fibronectin adsorbed onto hydrophobic as compared to hydrophilic tissue culture plates (13).

Although this work is preliminary and definitive conclusions cannot be drawn, the results suggest that: (1) human plasma fibronectin is adsorbed differently onto the two surfaces examined; (2) its adsorption and desorption behavior is a function of local solution hydrodynamics; and (3) that intrinsic UV TIRF is a useful method to probe microenvironmental effects and possibly conformational changes upon adsorption.

ACKNOWLEDGMENTS

This work has been supported in part by NIH Grant HL 18519. The assistance of Ms. Wendy Hopson and Mr. Jeff Geisler and discussions with Dr. F. Grinnell, Dr. S. W. Kim, and Dr. D. E. Gregonis are noted and appreciated.

REFERENCES

1. Mosher, D. F., *Prog. Hemost. Thromb.* **5**, 111 (1980).
2. Peterson, T. E., Thøgersen, N. C., Skorstengaard, K., Vibe-Petersen, K., Sahl, P., Sottrup-Jensen, L., and Magnusson, S., *Proc. Natl. Acad. Sci. USA* **80**, 137 (1983).
3. Kotliansky, V. E., Glukhova, M. A., Bejanien, M. V., Sminov, V. N., Filimanov, V. V., Zalite, O. M., and Venyaminov, S. Y., *Eur. J. Biochem.* **119**, 619 (1981).

4. Tooney, N. M., Arnrani, D. L., Homandberg, G. A., McDonald, J. A., and Moessan, M. W., *Biochem. Biophys. Res. Commun.* **108**, 1085 (1982).
5. Alexander, S. S., Colonna, G., and Edelhoch, H., *J. Biol. Chem.* **254**, 1501 (1979).
6. Odermatt, E., Engel, J., Richter, H., and Hormann, H., *J. Mol. Biol.* **159**, 109 (1982).
7. Engel, J., Odermatt, E., Engel, A., Madri, J. A., Furthmayr, W., Rohde, H., and Timpl, R., *J. Mol. Biol.* **150**, 97 (1981).
8. Price, T. M., Rudee, M. L., Pierschbacher, M., and Rouslohti, E., *Eur. J. Biochem.* **129**, 359 (1982).
9. Vario, T., and Vaheri, A., *Trends Biol. Sci.* **8**, 442 (1983).
10. Rocco, M., Hantger, R. R., Hermans, J., and McDonogh, J., *Circulation* **66** (Suppl. II), 320 (1982).
11. Williams, E. C., Janmey, P. A., Ferry, J. D., and Mosher, D. F., *J. Biol. Chem.* **257**, 14973 (1982).
12. Hughes, R. C., Pena, S. D. J., Clark, J., and Dourmashkin, R. R., *Exp. Cell Res.* **121**, 307 (1979).
13. Grinnell, F., and Feld, M. K., *J. Biol. Chem.* **257**, 4888 (1982).
14. Klebe, R. J., Bentley, K. L., and Schoen, R. C., *J. Cell. Pathol.* **109**, 481 (1981).
15. Young, B. R., Lambrecht, L. K., Cooper, S. L., and Mosher, D. F., "Biomaterials: Interfacial Phenomena and Applications," ACS Advances in Chemistry Series **199** (S. L. Cooper and N. A. Peppas, Eds.), p. 317. Amer. Chem. Soc., Washington, D. C., 1982.
16. Jönsson, U., Ivarsson, B., Lundström, I., and Berghem, L., *J. Colloid Interface Sci.* **90**, 148 (1982).
17. Adams, G. A., and Feuerstein, I. A., *Trans. Amer. Soc. Artif. Intern. Organs* **27**, 219 (1981).
18. Koltisko, B. M., Jr., thesis, Case Western Reserve University, Cleveland, 1981.
19. Haas, R., and Culp, L. A., *J. Cell. Physiol.* **113**, 289 (1982).
20. Mosher, D. F., and Johnson, R. B., *J. Biol. Chem.* **258**, 6595 (1983).
21. Van Wagenen, R. A., Rockhold, S., and Andrade, J. D., in "Biomaterials: Interfacial Phenomena and Applications" ACS Advances in Chemistry Series **199** (S. L. Cooper and N. A. Peppas, Eds.), p. 351. Amer. Chem. Soc., Washington, D. C., 1982.
22. Rockhold, S. A., Quinn, R. D., Van Wagenen, R. A., and Andrade, J. D., *J. Electroanal. Chem.* **150**, 261 (1983).
23. Lok, B. K., Cheng, Y.-L., and Robertson, C. R., *J. Colloid Interface Sci.* **91**, 87 (1983).
24. Hlady, V., Van Wagenen, R. A., and Andrade, J. D., in "Protein Adsorption" (J. D. Andrade, Ed.), Plenum, in press.
25. Smith, L., Doyle, C., Gregonis, D. E., and Andrade, J. D., *J. Appl. Polym. Sci.* **26**, 1269 (1982).
26. Haller, I., *J. Amer. Chem. Soc.* **100**, 8050 (1978).